https://doi.org/10.5194/egusphere-2025-6306
Preprint. Discussion started: 28 December 2025

A quasi-Lagrangian perspective on the role of dry and moist processes in the formation of blocked North Atlantic-European weather regimes

Seraphine Hauser[1,2], Franziska Teubler[3], Michael Riemer[3], and Christian M. Grams[2,4]

[1]Institute for Atmospheric and Climate Science, ETH Zurich, Zurich, Switzerland
[2]Institute of Meteorology and Climate Research (IMKTRO), Department Troposphere Research, Karlsruhe Institute of Technology (KIT), Karlsruhe, Germany
[3]Institute for Atmospheric Physics, Johannes Gutenberg-University Mainz, Mainz, Germany
[4]Federal Institute of Meteorology and Climatology, MeteoSwiss, Zurich-Flughafen, Switzerland

Correspondence: Seraphine Hauser (seraphine.hauser@env.ethz.ch)

Abstract.

Atmospheric blocking often triggers extreme events and remains difficult for weather and climate models to represent due to the complex multi-scale processes in its lifecycle. While recent studies highlight the importance of latent heat release in building and maintaining the upper-level anticyclonic anomaly, different perspectives assign varying roles to dry and moist dynamics, and it is still unclear whether their relative roles differ across regions where blocking occurs. This study uses a quasi-Lagrangian potential vorticity (PV) framework applied to ERA5 (1979–2021) to investigate blocking in the North Atlantic-European sector from the perspective of four large-scale blocked weather regimes. We track negative upper-tropospheric PV anomalies ($PVAs^-$) around blocked regime onset and quantify the processes governing their amplitude changes to assess the roles of dry and moist dynamics. Most $PVAs^-$ linked to blocked regime onset are not formed in situ but follow two main pathways, arriving either from upstream or from downstream. $PVAs^-$ intensify in the days before onset, with moist, divergence-related PV tendencies associated with warm conveyor belt activity and baroclinic PV tendencies contributing strongly to their amplification, independent of blocked regime type or pathway. The position of $PVAs^-$ relative to storm tracks determines the strength of the moist contribution, with moist processes exerting a greater influence within the midlatitude storm track over the North Atlantic. Consequently, the magnitude of PVA^- amplification depends more on whether a PVA^- arrives from upstream or downstream, since the pathway controls the timing, location, and strength of the moist-dynamical processes acting on it, than on the blocked regime type it eventually contributes to. This study highlights the synoptic-scale moist-dynamical evolution of $PVAs^-$ associated with different types of blocked regimes from a quasi-Lagrangian perspective. Complementing the quasi-Lagrangian analysis with previous insights from a Eulerian perspective provides a coherent view of blocked regime evolution, linking the remote moist amplification of $PVAs^-$ with the local formation of the regime pattern by anomaly re-arrangement, which is dominated by dry, quasi-barotropic dynamics. Given the key role of moist processes in PVA^- amplification and the systematic biases of blocking in weather and climate models, our results emphasize the need for better representation of moist baroclinic eddies and scale interactions, from cloud microphysics to the synoptic scale.

https://doi.org/10.5194/egusphere-2025-6306
Preprint. Discussion started: 28 December 2025

1 Introduction

Atmospheric blocking is a large-scale, persistent circulation pattern characterized by a quasi-stationary high-pressure system that disrupts the westerly flow in midlatitudes (Rex, 1950) and is often linked to prolonged periods of anomalous weather conditions such as heatwaves, cold spells, or droughts (see review article by Kautz et al., 2022). While numerical weather prediction (NWP) models have made significant progress in recent decades (e.g., Davini and D'Andrea, 2016), accurately predicting blocking events still remains challenging due to its non-linear and chaotic nature (Ferranti et al., 2015). Variations in blocking characteristics across regions, particularly between the North Atlantic and Pacific sectors, influence regional predictability and impact numerical weather prediction and climate projections. Especially in the North Atlantic-European sector, many climate models underestimate the frequency and duration of blocking (e.g., Quinting and Vitart, 2019; Woollings et al., 2018; Davini and D'Andrea, 2016; Maddison et al., 2024).

Understanding the development of blocking patterns is key to improving predictions of blocking events. Existing theories on blocking focus on (i) large-scale wave dynamics (Austin, 1980), (ii) the role of topography in the initiation of blocking on the planetary scale (e.g., Grose and Hoskins, 1979), (iii) wave resonance to a given forcing (e.g., Petoukhov et al., 2013), (iv) the impact of tropical heating (e.g., Henderson et al., 2016), (v) the formation of atmospheric "traffic jams" in terms of wave-activity concepts (e.g., Nakamura and Huang, 2018; Polster and Wirth, 2023), (vi) the effect of transient activity such as upstream cyclones (e.g., Nakamura and Wallace, 1990, 1993), (vii) the absorption of eddies by a block as maintenance mechanism (e.g., Shutts, 1983; Yamazaki and Itoh, 2009; Suitters et al., 2023), (viii) the non-linear interaction and feedbacks between small-scale eddies with a block (e.g., Luo et al., 2014), and (ix) the effect of diabatic processes in modifying the upper-level flow in the troposphere (e.g., Pfahl et al., 2015; Steinfeld and Pfahl, 2019; Lubis et al., 2025). The effect of moist-diabatic processes received much attention in recent years, which often focuses on warm conveyor belts (WCBs), i.e., the rapidly ascending airstreams in the vicinity of extratropical cyclones. From a Lagrangian air-parcel perspective, previous studies highlighted moist dynamics as first-order importance for the onset and maintenance of atmospheric blocking (Wernli, 1997; Madonna et al., 2014; Pfahl et al., 2015). Numerical studies support this hypothesis, showing that omitting latent heat release in "dry simulations" weakens or suppresses blocking and can fundamentally alter its characteristics (Steinfeld et al., 2020; Deshmukh et al., 2025). Blocking is a complex, non-linear scale-interaction phenomenon involving interactions across scales and both dry and moist processes, and despite progress in recent years, a comprehensive understanding of its life-cycle dynamics remains elusive.

Given regional differences in blocking predictability, recent studies have quantified how blocking occurrences and dynamics vary by location. Distinct onset mechanisms are observed over the Atlantic, Europe, Asia, and the Pacific, which are linked to different frequency bands of atmospheric flow (Miller and Wang, 2022), with Pacific blocks influenced by intermediate-frequency processes and Atlantic and European blocks dominated by low- and high-frequency processes, respectively. Baroclinic energy conversion is particularly efficient for blocks over the Bering Sea and near Greenland, but less important for blocks over the Eastern Atlantic (Martineau et al., 2022). The contribution of diabatic heating to blocking formation and maintenance is pattern-dependent (Liu and Wang, 2025) and further varies with region and season (Steinfeld and Pfahl, 2019;

https://doi.org/10.5194/egusphere-2025-6306
Preprint. Discussion started: 28 December 2025

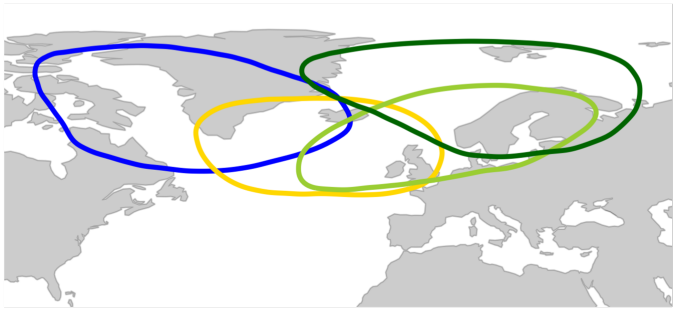

(a)

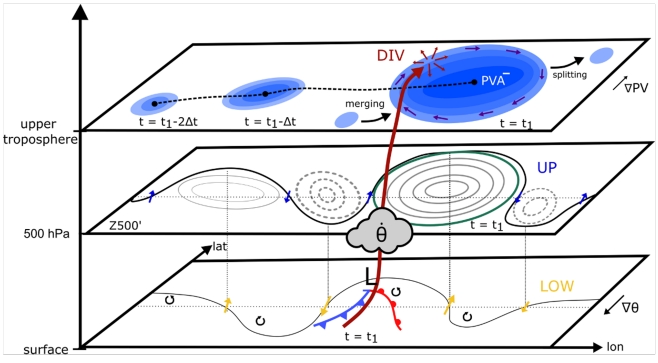

(b)

Figure 1. (a) Subregions for blocking in the North Atlantic–European sector obtained from a weather regime perspective. The solid, closed contour lines mark the areas of the anticyclonic PV anomaly associated with the blocked regime patterns: Atlantic Ridge (gold), European Blocking (yellow-green), Scandinavian Blocking (dark green), and Greenland Blocking (blue). (b) Schematic of the quasi-Lagrangian potential vorticity framework (Hauser et al., 2023, 2024b). Upper-troposphere level: Exemplary track (black dashed) of negative PV anomalies (blue shading, PVA^{-}), including splitting and merging of existing anomalies; impact of divergent outflow near the tropopause (DIV, dark-red arrows); and wind fields induced by upper-tropospheric PV anomalies (dark-blue arrows). 500 hPa level: absolute geopotential height (Z500; black), Z500 anomalies ($Z500'$; grey; solid for positive, dashed for negative), contour of the anticyclonic anomaly as in panel (a) (green), and wind fields linked to barotropic phase-propagation tendencies (UP, blue arrows). Surface: temperature wave (solid black line), influence of wind fields linked to low-level PV anomalies on higher levels (LOW, gold arrows), symbolic low-pressure system (L) with cold (blue) and warm (red) fronts, and a warm-conveyor-belt airstream (dark-red arrow) with diabatic heating in the mid-troposphere (grey cloud).

Drouard et al., 2021). Oceanic blocks show consistently high influence, while continental blocks, especially over Asia, exhibiting strong seasonality. Polar and European blocks are generally dominated by dry dynamics, and delayed latent heat signals in Arctic and European blocks indicate upstream diabatic heating days before onset (Steinfeld and Pfahl, 2019). Very long-lived blocks occur mostly in high latitudes over Greenland and the North Pacific and are favoured by cyclonic Rossby wave breaking and maintained by transient local mechanisms upstream (Drouard et al., 2021). These results provide a first assessment of regional differences in blocking dynamics, highlighting the need to further refine spatial scales to understand why blocking in the North Atlantic–European domain remains challenging for weather and climate models.

https://doi.org/10.5194/egusphere-2025-6306
Preprint. Discussion started: 28 December 2025

Different blocking patterns over the North Atlantic–European sector have mainly been examined through large-scale weather regimes. The year-round regime definition of Grams et al. (2017), comprising seven regimes, has been widely used to analyse the predictability (Büeler et al., 2021; Osman et al., 2023) and dynamics (e.g., Hauser et al., 2023; Teubler et al., 2023; Hauser et al., 2024b; Wandel et al., 2024) of the four different blocked regime types (Figure 1a), namely the Atlantic ridge (AR), European blocking (EuBL), Scandinavian blocking (ScBL), and Greenland blocking (GL). EuBL and ScBL exhibit the lowest forecast skill, while GL shows comparatively high skill (Büeler et al., 2021; Osman et al., 2023), consistent with dynamical-systems-theory evidence that GL features enhanced stability and persistence whereas EuBL and ScBL rank among the least stable regimes (Faranda et al., 2016; Hochman et al., 2021). Forecast performance for EuBL depends on capturing upstream WCB activity, underscoring the role of moist dynamics in blocking onset (Wandel et al., 2024), and model biases in WCB outflow frequency have been linked to the underestimation of winter blocking over the eastern North Atlantic and Europe (Dolores-Tesillos et al., 2024). From a Eulerian perspective, low-frequency streamfunction-tendency and pattern-projection analyses revealed the importance of wave trains from the western Atlantic and the absence of Rossby wave breaking over western Europe as precursors to blocking (e.g., Feldstein, 2002; Michel and Rivière, 2011; Drouard and Woollings, 2018). Building on this, Teubler et al. (2023) applied a PV-based projection framework to the four blocked regimes of Grams et al. (2017) to diagnose processes that locally reinforce or erode the respective anomaly patterns, highlighting the predominant influence of in-situ dry-dynamical processes in the formation of blocked regimes.

In a case study, Hauser et al. (2023) demonstrate that assessing the relative importance of moist processes in blocking development depends systematically on the diagnostic framework and argue that a combination of complementary perspectives provides a more holistic understanding of blocking dynamics. The current study employs a quasi-Lagrangian approach, which arguably provides the most important complementary perspective to a Eulerian approach. Specifically, we use the quasi-Lagrangian PV framework introduced in Hauser et al. (2023) (here illustrated schematically in Figure 1b). This framework tracks negative PV anomalies linked to blocking (hereafter referred to as PVAs$^-$), thereby providing the important information of the (spatial) origin of involved PVAs$^-$. In addition, the processes governing the amplitude evolution of PVAs$^-$ are evaluated, enabling an assessment of the relative importance of dry and moist processes. The separation into different processes is done by decomposing the total change in PV into (i) linear, quasi-barotropic Rossby wave dynamics, (ii) baroclinic interaction, and (iii) divergent outflow. Hauser et al. (2024b) applied the quasi-Lagrangian framework to systematically investigate GL regime life cycles and showed that PVAs$^-$ associated with blocked-regime onset originate primarily upstream and downstream of the blocking region rather than forming in situ. Their analysis also highlighted the importance of moist processes in the growth of PVAs$^-$ prior to blocked regime onset. A synopsis of the dynamics of all four blocked regimes from a quasi-Lagrangian perspective, as a vital contribution to understanding the processes that initiate and maintain blocking patterns in the North Atlantic-European region, however, is still missing.

In this study, the quasi-Lagrangian framework is applied to the four year-round blocked regime types over the North Atlantic-European region of Grams et al. (2017) for the period 1979 to 2021. With a very similar interpretation of the governing processes, and considering the same blocked regime types over the same time period, the results of the current study are directly comparable to those of Teubler et al. (2023). Building on these results, and on the new insight offered by the quasi-

https://doi.org/10.5194/egusphere-2025-6306
Preprint. Discussion started: 28 December 2025

Lagrangian framework, the current study can thus provide, for the first time, a more holistic understanding across a large number of cases by combining two complementary perspectives. With this synopsis, the study addresses the following key questions:

- Where do PVAs$^-$ linked to blocked regimes develop (upstream, downstream, locally) and is the propagation of those PVAs$^-$ linked to certain regime transitions?
- How do processes (dry vs. moist) differ in the evolution of PVAs$^-$ between the blocked regimes and possible pathways of PVAs$^-$?
- Is the contribution of moist processes dependent on the location of the PVA$^-$ relative to the storm track region?
- How can we optimally combine different perspectives to yield a holistic view of the relevance of local versus non-local effects of processes involved in blocked regime onsets?

The paper is structured as follows: Section 2 describes the datasets and methods used in this study. Section 3 presents the results, divided into five subsections. This is followed by the discussion in Section 4 and concluding remarks in Section 5.

2 Data and methods

2.1 ERA5 reanalysis dataset

The analyses presented in this study are based on the ERA5 reanalysis from the European Centre for Medium-Range Weather Forecasts (ECMWF) and covers the period 1 January 1979 to 31 December 2021 (Hersbach et al., 2020). We use 3-hourly model level data provided by ECMWF for a high-resolution computation of PV anomalies in the upper troposphere (see Section 2.3) on a 0.5° x 0.5° latitude-longitude grid, and a coarser dataset (1° x 1°) for the PV inversion (Teubler and Riemer, 2021) on 17 pressure levels (1000, 950, 925, 900, 850, 800, 700, 600, 500, 400, 300, 250, 200, 150, 100, 70, and 50 hPa).

2.2 Quasi-Lagrangian potential vorticity framework

The quasi-Lagrangian PV framework, developed by Hauser et al. (2023) and further refined in Hauser et al. (2024b), identifies and tracks patches of negative PV anomalies in the upper troposphere and quantifies the contribution of different processes to their amplitude evolution. This approach builds on the θ-PV framework for midlatitude Rossby wave packets by Teubler and Riemer (2016). The central variable is Ertel potential vorticity (PV), defined by Ertel (1942): $q = -g(\zeta_\theta + f)\frac{\partial \theta}{\partial p}$, where g is the gravitational acceleration, ζ_θ the isentropic relative vorticity, f the Coriolis parameter, θ the potential temperature, and p the pressure. The full framework is documented in detail in Hauser et al. (2024b); here, we briefly summarize the key steps only to avoid redundancy.

Upper-tropospheric PV anomalies are defined as the difference between the vertically averaged PV (VAPV) between 150 and 500 hPa and its 30-day centred running-mean climatology (1979–2021). Negative PV anomaly patches, referred to as PVAs$^-$,

https://doi.org/10.5194/egusphere-2025-6306
Preprint. Discussion started: 28 December 2025

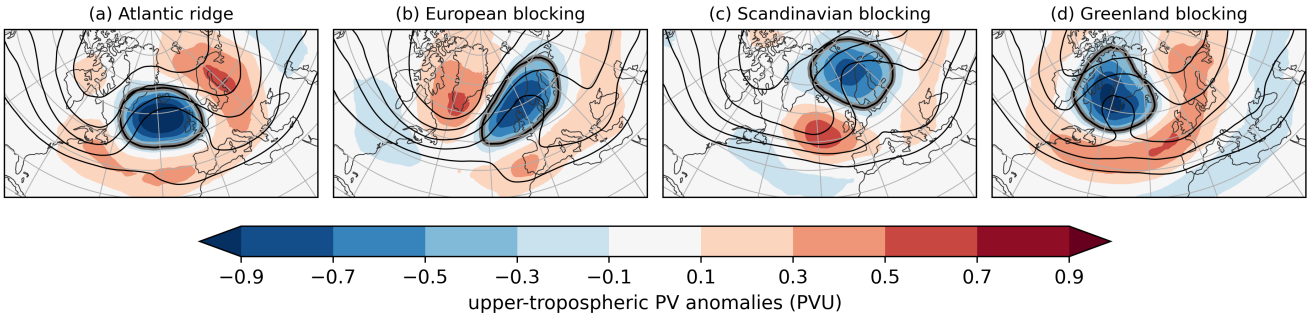

Figure 2. Composites of vertically-averaged PV anomalies between 500–150 hPa (shading) and vertically-averaged PV for all time steps attributed to each of the four blocked regime types (contours, in PVU, from 1.5 to 3.5 PVU in steps of 0.5 PVU). The thick black contour illustrates the regime mask for the respective regime type, defined by the -0.3 PVU contour.

are identified as contiguous regions of negative PV anomalies that fall below a seasonally varying threshold (cf. Hauser et al., 2024b, their Figure A1c), with higher thresholds in winter than in summer. All PVAs$^-$ are tracked using an overlap-based tracking algorithm, which also handles splitting and merging events appropriately. The dataset of tracked PVAs$^-$ within the chosen ERA5 period (1979–2021) is available for the entire Northern Hemisphere in Hauser et al. (2024a).

To investigate the amplitude evolution of PVAs$^-$, we employ the piecewise PV tendency framework, which is based on the PV tendency equation. This equation states that the local change in PV (q) is governed by PV advection and non-conservative PV modification:

$$\frac{\partial q}{\partial t} = -\mathbf{v}\cdot\boldsymbol{\nabla}_\theta q + \mathcal{N} = -(\mathbf{v}_0 + \mathbf{v}'_{div} + \mathbf{v}'_{up} + \mathbf{v}'_{low} + \mathbf{v}'_{res})\cdot\boldsymbol{\nabla}_\theta q + \mathcal{N}. \tag{1}$$

Here, $\mathbf{v}$ is the horizontal wind field $\mathbf{v} = (u, v, 0)$, $\boldsymbol{\nabla}_\theta$ the gradient operator along an isentropic surface, and $\mathcal{N}$ the non-conservative PV modification. The full wind field $\mathbf{v}$ is decomposed using PV inversion (Davis and Emanuel, 1991; Davis, 1992) and Helmholtz Partitioning, which results in the divergent wind field $\mathbf{v}'_{div}$, the wind fields $\mathbf{v}'_{low}$ and $\mathbf{v}'_{up}$ associated with upper-tropospheric and lower-tropospheric PV anomalies (non-divergent), the residual wind field $\mathbf{v}'_{res}$, and the background wind field $\mathbf{v}_0$, defined as the 30-day running mean climatology of $\mathbf{v}$ (1980–2019). Equation 1 is further transformed into an equation for the amplitude evolution of enclosed PV anomalies – analogously to Hauser et al. (2024b). As a result, the integrated amplitude evolution over the area $A(t)$ of a PV anomaly feature reads as

$$\begin{aligned}\frac{d}{dt}\int_{A(t)} q'\,dA = \sum_i \underbrace{-\int_{A(t)} \mathbf{v}'_i\cdot\boldsymbol{\nabla}q_0\,dA - \int_{A(t)} \langle -\mathbf{v}'_i\cdot\boldsymbol{\nabla}q_0\rangle\,dA}_{i} + \underbrace{\int_{A(t)} q'(\boldsymbol{\nabla}\cdot\mathbf{v}'_{div})\,dA - \int_{A(t)} \langle q'(\boldsymbol{\nabla}\cdot\mathbf{v}'_{div})\rangle\,dA}_{\mathrm{DIV}_{div}} \\ + \underbrace{\int_{A(t)} \mathcal{N}\,dA - \int_{A(t)} \mathcal{N}_0\,dA}_{\mathrm{NONCONS}} + \underbrace{\oint_{S(t)} q'(\mathbf{v}_s - \mathbf{v})\,d\mathbf{S}}_{\mathcal{B}nd},\end{aligned} \tag{2}$$

https://doi.org/10.5194/egusphere-2025-6306
Preprint. Discussion started: 28 December 2025

with i referring to *div up*, *low* and *res* wind fields (cf. Equation 1), $S(t)$ as the boundary of $A(t)$, $\mathbf{v}_s$ the motion of the boundary $S(t)$ and the climatological background PV q_0 which is constructed the same way as $\mathbf{v}_0$. The terms enclosed by the mean operator <> refer to 30-day centred averages of a given term between 1980–2019 for each calendar day. Taking into account these terms, we can quantify the contributions of different processes to the change in background PV (Hauser et al., 2024b, their Appendix A). Equations 1 and 2 are evaluated on isentropic surfaces ranging from 315 K to 355 K in steps of 5 K. Following the approach of Teubler et al. (2023) and Hauser et al. (2024b), we compute an isentropic average by including the surfaces ±5 K around the central level. For the year-round analysis of PVAs$^-$, the selection of the representative isentropic level is crucial. Therefore, we adopt the seasonally varying levels recommended by Röthlisberger et al. (2018): 320 K for December to March, 325 K for April and November, 330 K for May and October, 335 K for June and September, and 340 K for July and August.

The physical meaning of each term in Equation 2 is explained below and schematically shown in Figure 1b. The term **UP** refers to upper-tropospheric (quasi-)barotropic dynamics and describes the advection of upper-level background PV by the wind field associated with upper-tropospheric PV anomalies (e.g., Hoskins et al., 1985, Section 6a). This describes the intrinsic propagation mechanism of Rossby waves and amplitude changes due to group propagation (blue arrows in Figure 1b). The term **LOW** captures baroclinic interaction, namely the amplitude modification of upper-level PV anomalies by the wind field associated with low-level PV anomalies (gold arrows in Figure 1b). LOW contributes to baroclinic growth, while still being largely considered a dry dynamical process, and its impact depends on the phase relationship between the upper-level PV wave and the lower-level temperature wave (e.g., Hoskins et al., 1985, Section 6b). Numerical and inherent inaccuracies in piecewise PV inversion lead to a residual wind field, which is usually small. The advection of background PV by this residual flow is captured by the term **RES**. While it lacks physical interpretability (Teubler and Riemer, 2016), it is included for budget closure in the PV tendency equation. Two terms describe the impact of divergent winds on the amplitude evolution of PV anomalies: (1) $\mathbf{DIV}_{\text{adv}}$ represents the advection of background PV by the divergent wind field and (2) $\mathbf{DIV}_{\text{div}}$ accounts for divergence or convergence within the PV anomaly itself, which leads to its growth or decay, respectively. Because large upper-level divergence is frequently associated with latent heat release below, such as in WCB outflow near the tropopause (e.g., Madonna et al., 2014; Pfahl et al., 2015; Hauser et al., 2023), both of these terms are considered indirect moist contributions (dark red arrows in Figure 1b). The term **NONCONS** represents direct diabatic modification of PV due to non-conservative processes such as latent heating, radiative effects, friction, and turbulent mixing (e.g., Chagnon et al., 2013). However, this term—except of radiative PV tendencies which however show little spatio-temporal variability over the life cycle of PV anomalies (Teubler and Riemer, 2021)—is often small in the area-integrated perspective due to its localized structure. Following Teubler and Riemer (2021) and Hauser et al. (2024b), NONCONS is not considered further in this study.

The final term on the right-hand side of Equation 2 is the boundary term $\boldsymbol{\mathcal{Bnd}}$, that is estimated as follows:

$$\mathcal{B}nd = -\int_{A(t)} \boldsymbol{\nabla}\cdot(\mathbf{v}q')\,dA - \int_{A(t)} <-\boldsymbol{\nabla}\cdot(\mathbf{v}q')>\,dA + \overline{q}'\cdot\Delta A \tag{3}$$

https://doi.org/10.5194/egusphere-2025-6306
Preprint. Discussion started: 28 December 2025

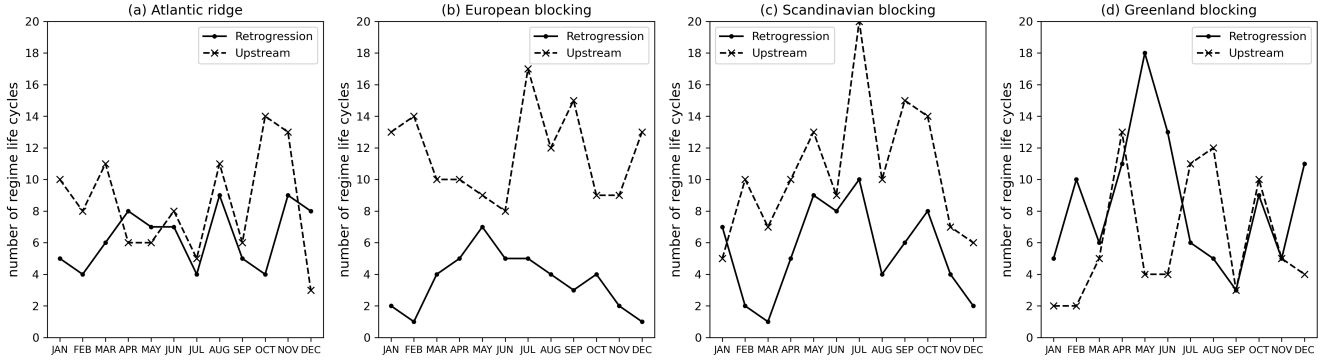

Figure 3. Monthly distribution of the absolute number of regime life cycles for the two identified pathways for each of the four blocked regimes. The retrogression pathway is shown with a solid line, and the upstream pathway with a dashed line.

with $\overline{q}$ as the average of q' along the boundary $S(t)$ and $\Delta\mathcal{A}$ as the observed area change of the PV anomaly. The first two terms of $\mathcal{B}$nd describe the contribution to amplitude change caused by eddy flux divergence or convergence within the anomaly area. The last term estimates the change in amplitude by the change in anomaly area between two consecutive time steps and can reach high values in case of slitting and merging of different anomaly features. For more details on $\mathcal{B}$nd, the reader is referred to Appendix B of Hauser et al. (2024b).

We refer to the diagnosed amplitude change (DIAG) as the sum of all terms in Equation 2: DIAG = UP + LOW + DIV_{div} + DIV_{adv} + RES + $\mathcal{B}$nd. DIAG is compared to the observed amplitude change (OBS), which is defined as the forward difference in the area-integrated PV anomaly amplitude between two time steps. Following Hauser et al. (2024b), we exclude time steps where the deviation between DIAG and OBS is large, as this indicates that the PV budget (DIAG) fails to accurately capture the observed evolution. In line with Teubler and Riemer (2016), the sign convention for the PV tendency terms is such that a positive value indicates an amplification of PVAs^{-}, while a negative value indicates a weakening.

2.3 Year-round definition of North Atlantic-European weather regimes

In this study, we use the year-round weather regime definition for the North Atlantic–European region developed by Grams et al. (2017) and apply it to ERA5 reanalysis data to distinguish between different blocking configurations in this region. To define the regimes, 6-hourly geopotential height anomalies at 500 hPa (Z500) are calculated using a 90-day centred running-mean climatology (1979–2019) and then filtered with a 10-day low-pass Lanczos filter (Duchon, 1979). After normalizing the anomalies, we perform an empirical orthogonal function (EOF) analysis over the North Atlantic–European domain (80°W–40°E, 30°–90°N). The seven leading EOFs, which describe 74.4 % of the total variance, are retained to construct an expanded phase space. A k-means clustering is then applied in this phase space, yielding an optimal number of seven clusters, which correspond to seven distinct weather regimes: Three cyclonic regimes (Zonal regime – ZO, Scandinavian trough – ScTr, Atlantic trough – AT) and four anticyclonic regimes (Atlantic ridge – AR, European blocking – EuBL, Scandinavian blocking – ScBL, Greenland blocking – GL). To assign individual time steps to these regimes, we use the weather regime index (I_{WR})

https://doi.org/10.5194/egusphere-2025-6306
Preprint. Discussion started: 28 December 2025

proposed by Michel and Rivière (2011) and Grams et al. (2017), which quantifies the similarity between a given instantaneous Z500 field at time t and each of the seven weather regimes (WR):

$$I_{WR}(t) = \frac{P_{WR}(t) - \overline{P_{WR}}}{\sqrt{\frac{1}{NT}\sum_{t=1}^{NT}[P_{WR}(t) - \overline{P_{WR}}]^2}} \tag{4}$$

with

$$P_{WR}(t) = \frac{\sum_{(\lambda,\varphi)\in EOF} \Phi^L(t,\lambda,\varphi)\Phi^L_{WR}(\lambda,\varphi)\cos\varphi}{\sum_{(\lambda,\varphi)\in EOF}\cos\varphi}. \tag{5}$$

$P_{WR}(t)$ describes the projection of the filtered anomaly $\Phi^L(t,\lambda,\varphi)$ to the EOF cluster mean $\Phi^L_{WR}(\lambda,\varphi)$ within the EOF domain. NT is the total number of time steps within the climatological sample (1979–2019) and the respective longitude/latitude within the EOF domain is noted as (λ,φ). $\overline{P_{WR}}$ describes the climatological mean of the projection P_{WR}. As a result, I_{WR} is computed as the deviation of $P_{WR}(t)$ from $\overline{P_{WR}}$, normalized by the standard deviation. This index, I_{WR}, can also be computed beyond the climatological sample—i.e., for each of the seven regimes and every 3-hourly time step throughout the full ERA5 period considered (1979–2021). Following Grams et al. (2017), we derive objective regime life cycles, associated life cycle stages (onset, mature stage, decay) and regime transitions – all based on the I_{WR}. A detailed description on the algorithms used to determine those characteristics is given in Hauser et al. (2024b).

From January 1979 to December 2021, we identified a total of 177 life cycles for AR, 183 for EuBL, 192 for ScBL, and 177 for GL. Figure 2 presents the four blocked regime patterns as year-round mean composites based on upper-tropospheric PV anomalies and calculated over all time steps within the respective life cycles of each blocked regime. All four regimes are characterized by a dominant negative PV anomaly that defines the block; however, the location of this anomaly varies across regimes. For AR, the negative PV anomaly spans the largest area and is centred south of Iceland (Figure 2a). A comparison between EuBL and ScBL highlights the need to refine the classical four-regime blocking framework (e.g., Vautard, 1990; Michelangeli et al., 1995) by distinguishing these two as separate sub-regimes due to their markedly different spatial structures. EuBL exhibits a pronounced positive PV anomaly over Greenland and displays features indicative of anticyclonic Rossby wave breaking over Europe (Figure 2b). In contrast, ScBL is associated with a high-latitude block flanked by a strong positive PV anomaly over the eastern North Atlantic, and shows signs of cyclonic Rossby wave breaking extending toward Greenland (Figure 2c). For GL, the block is associated with a more isolated negative PV anomaly centred over the Labrador Sea (Figure 2d).

2.4 Eulerian identification of warm conveyor belts

This work utilizes the EuLerian Identification of ascending AirStreams (ELIAS 2.0) data set of Quinting and Grams (2022). ELIAS 2.0 uses convolutional neural networks (CNNs) to identify the footprints of three WCB stages, which have been defined from a Lagrangian perspective based on the location of air parcels that classify as WCB ($\Delta p > 600\,\text{hPa}$ for $\Delta t \leq 48$ hours; Madonna et al., 2014): (i) inflow ($p \geq 800\,\text{hPa}$), (2) ascent ($800\,\text{hPa} \leq p \leq 400\,\text{hPa}$), and (3) outflow ($p \leq 400\,\text{hPa}$). A stepwise forward selection approach has been applied to identify the five most important meteorological predictors (Quinting and

https://doi.org/10.5194/egusphere-2025-6306
Preprint. Discussion started: 28 December 2025

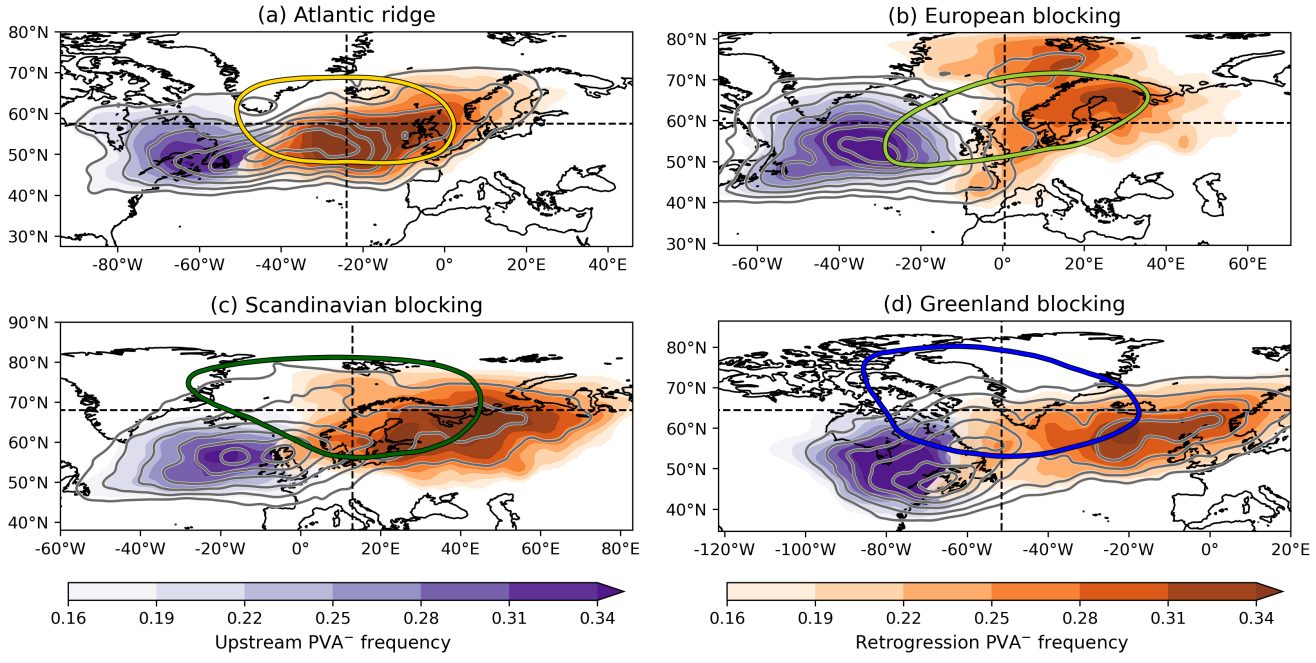

Figure 4. Mean composites (shading) of onset PVA$^-$ frequency for the two different pathways (orange colours for retrogression pathway, violet colours for upstream pathway) at t = -72 h before blocked regime onset for the four blocked regimes. The shading represents the onset PVA$^-$ frequency within each respective pathway subset. The data is smoothed by taking into account the time steps +/- 6 hours around t = -72 h and using a Gaussian filter with σ = 2. Grey contours show the total onset PVA$^-$ frequency, independent of pathway (0.1 to 0.4 in increments of 0.03). Coloured closed contours mark the regime masks (same as in Figure 2). Dashed black vertical and horizontal lines indicate the centre of mass position of the regime mask, which is used to separate the two pathways.

Grams, 2021). The training has been performed on 6-hourly ERA-Interim data (Dee et al., 2011) and applied to 3-hourly ERA5 data. The CNN gives conditional probabilities of WCB stage occurrences as output. This is transformed into a binary WCB occurrence given a seasonal-dependent and grid-point-dependent decision threshold, optimized to minimize the climatological bias and maximize the correlation coefficient in the midlatitude storm-track regions, where WCBs occur most frequently (Madonna et al., 2014).

3 Results

3.1 Pathways of PVAs$^-$ to blocked regime onset

The negative upper-level PV anomaly linked to blocked regime onset over Greenland does not develop in-situ but propagate via different pathways towards Greenland (Hauser et al., 2024b). Consistent with the results, we distinguish two pathways based on whether the anomaly emerges upstream or downstream of the blocking region and examine if these pathways also

https://doi.org/10.5194/egusphere-2025-6306
Preprint. Discussion started: 28 December 2025

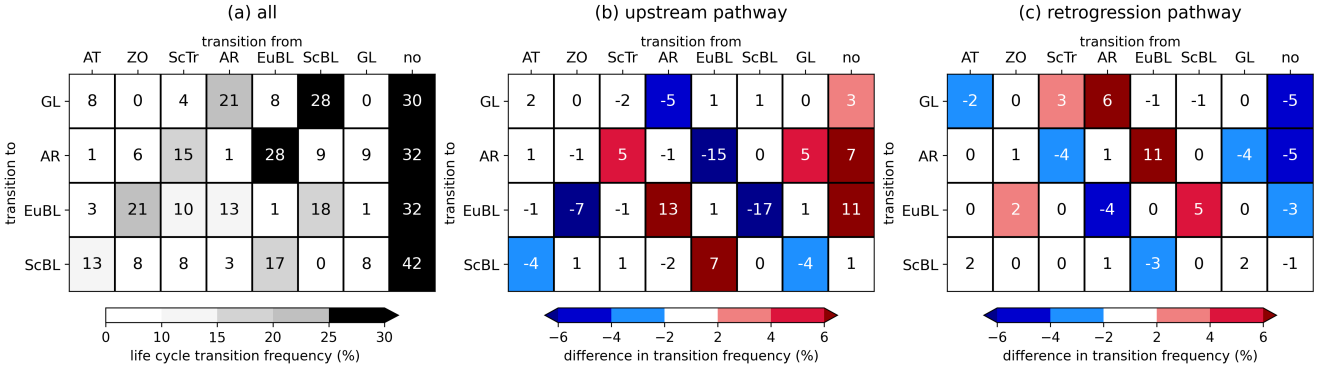

Figure 5. (a) Life cycle transition frequency (%) for all transitions into the blocked regimes (y-axis) from one of the seven regimes or the no regime (x-axis). (b) Differences in transitions frequency for the life cycles linked to the upstream pathway in comparison to all. (c) Differences in transitions frequency for the life cycles linked to the retrogression pathway in comparison to all.

exist in the remaining three blocked regimes. First, we define the area where to expect the anticyclonic anomaly during the blocked regimes by the −0.3 PVU-contour in the year-round composite (Figure 2). Using the traced PVAs$^-$ (details in Section 2.2), for every blocked regime life cycle, we determine a so-called onset PVA$^-$ that exhibits the highest spatial overlap with the respective regime mask around blocked regime onset. To quantify the two pathways, each onset PVA$^-$ is assessed for its dominant position relative to the centre of mass longitude of the regime mask (0.5°E for EuBL, 13.0°E for ScBL, 24.0°W for AR, and 51.5°W for GL) in the three days before onset.

When split into the two pathways, the majority of onset PVAs$^-$ follow the upstream pathway: 76.5 % for EuBL, 65.6 % for ScBL, and 57.1 % for AR. This deviates from the dominant retrogression pathway for GL, where upstream onset PVAs$^-$ account for only 42.4 %. These findings are consistent with the climatological storm-track position, characterized by reduced storm-track activity downstream of Europe and upstream of Greenland. Investigating the seasonal occurrence of the pathways reveals more differences between the blocked regimes (Figure 3). First, the more continental blocked regime types east of the North Atlantic (EuBL, ScBL) show a dominance of the upstream pathway mostly independent of the month (Figure 3b, c). The differences in pathway frequency are less pronounced for AR with a more frequent retrogression pathway in April, May and December (Figure 3a). The seasonality of the pathways for GL is more complex with the dominant retrogression pathway only being prevalent in winter and late spring/early summer (Figure 3a).

Figure 4 provides more insights into the position of onset PVAs$^-$ before blocked regime onset (grey contour lines). Apart from AR, onset PVAs$^-$ are located in the mean outside or at the edge of the blocking region three days before blocked regime onset, in particular in the southwest quadrant of the regime mask-centred composite (grey contour lines). This highlights the non-stationary development of PVAs$^-$ for multiple blocked regimes and extends the previous result found for GL by Hauser et al. (2024b). Although most GL life cycles are assigned to the retrogression pathway, the maximum in onset PVA$^-$ frequency is located southwest of the blocking domain (Figure 4d), suggesting a more confined pathway of upstream onset PVAs$^-$ compared to retrograding onset PVAs$^-$.

https://doi.org/10.5194/egusphere-2025-6306
Preprint. Discussion started: 28 December 2025

Depending on the blocked regime type, onset PVAs$^-$ following a given pathway are located either over the ocean or over land in the days preceding blocked regime onset. Blocked regimes centred over the North Atlantic (Figure 4a,d) exhibit two oceanic pathways. In contrast, for the blocked regimes over Europe and Scandinavia (EuBL and ScBL), the retrogression pathways (orange shading) remain confined to continental areas, whereas the upstream pathways (violet shading) extend over the ocean (Figure 4b,c).

Onset PVAs$^-$ along the upstream pathways peak outside the regime mask for all blocked regime types, providing clear evidence that they do not evolve in situ. In contrast, the location of onset PVAs$^-$ along the retrogression pathway in the days before blocked regime onset—whether inside, outside, or partially covering the regime mask—depends on the blocked regime type. For AR, retrograding onset PVAs$^-$ already reside very centrally in the regime mask three days before onset (Figure 4a). The signal of retrograding onset PVAs$^-$ of EuBL is mixed given the low sample size (cf. Figure 3b), but reveals that PVAs$^-$ are distributed both within and outside of the regime mask to its northeast (Figure 4b). For ScBL and GL, most retrograding onset PVAs$^-$ are located at the eastern edge of the regime mask for ScBL, and outside, to the east of the mask for GL (Figure 4c,d). This means that, despite sharing the same temporal reference point (blocked regime onset), the timing at which onset PVAs$^-$ enter the blocking region differs not only between individual life cycles but also systematically between blocked regime types. To avoid conflating these differences in timing and evolution in an Eulerian composite framework, a quasi-Lagrangian perspective is particularly well suited here.

3.2 Link between pathways and regime transitions

About three days before blocked regime onset, certain regions with high onset PVA$^-$ frequency coincide with the location of the regime mask associated with another blocked regime type (Figure 4). This raises the broader question of whether the pathways of onset PVAs$^-$ are linked to preferred regime transitions. Figure 5a shows the climatological frequency of regime transitions for each of the four blocked regimes. All four blocked regimes can arise from any regime type, except for GL, which never transitions from ZO during 1979–2021. The no-regime state is the most frequent origin, accounting for 30-42 % of transitions to blocked regimes. When the seven regime types are grouped into cyclonic and blocked regime types, GL and AR most often evolve from other blocked regimes, with transition frequencies of 57 % and 46 %, respectively. After the no-regime state, the most common transitions are ScBL to GL and EuBL to AR. Interestingly, the second most frequent transition into EuBL originates from ZO, showing that cyclonic-to-blocked transitions, while not dominant, occur regularly.

A comparison of regime transitions between the pathways shows that the upstream pathway dominates for blocked regime life cycles that develop from none of the seven regimes (Figure 5b,c). This suggests that blocked regimes forming during periods of more transient large-scale flow are primarily associated with upstream PVAs$^-$. A clear relationship emerges between the pathways and specific regime transitions when considering transitions between blocked regimes. Transitions from blocked regimes whose regime mask is located downstream of the current regime are predominantly linked to the retrogression pathway. Conversely, when the regime mask of the previous blocked regime is located upstream, onset PVAs$^-$ tend to follow the upstream pathway. This relationship holds for all blocked-to-blocked transitions, except for the climatologically frequent ScBL-to-GL transition, for which both pathways occur with similar frequency. However, it has been shown that both pathways can

https://doi.org/10.5194/egusphere-2025-6306
Preprint. Discussion started: 28 December 2025

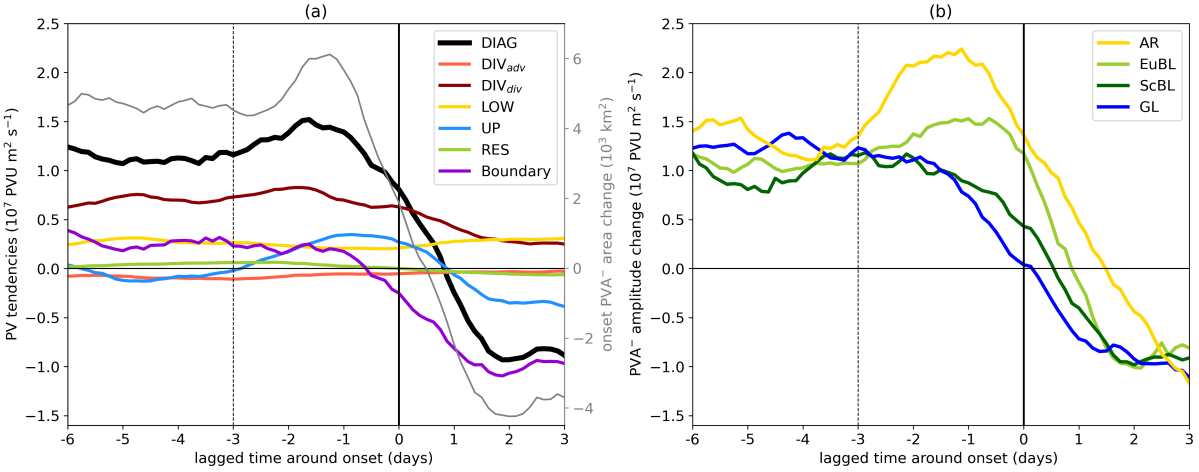

Figure 6. (a) Composite of amplitude-modifying contributions (left y-axis) to the diagnosed amplitude change of onset PVAs$^-$ (DIAG, black) for all blocked regime life cycles independent of type, following Equation 2: advection part of the divergent outflow term (DIV$_{adv}$, -$\mathbf{v}_{div} \cdot \nabla q_0$, light red), divergence part of the divergent outflow term (DIV$_{div}$, $q'(\nabla \cdot \mathbf{v}_{div})$, dark red), baroclinic interaction (LOW, -$\mathbf{v}_{up} \cdot \nabla q_0$, gold), upper-tropospheric wave dynamics (UP, -$\mathbf{v}_{up} \cdot \nabla q_0$, blue), the residual PV tendency term (RES, -$\mathbf{v}_{res} \cdot \nabla q_0$, yellow green) and the boundary term (Boundary, dark violet). The sign of the PV tendencies is defined such that positive (negative) values always indicate amplification (weakening) of the PVAs$^-$. They grey line shows the mean change in onset PVA$^-$ area (right y-axis).(b) Mean diagnosed amplitude change of onset PVAs$^-$ around blocked regime onset for the four blocked regimes separately. Note that all curves are smoothed by taking into account the time steps +/- 12 h.

occur at the same time, as multiple PVAs$^-$ propagate and trigger GL onset, with the onset PVA$^-$ merging with another PVA$^-$ along the alternative pathway Teubler et al. (2023).

Given the connection between pathways and regime transitions, we analyse whether the onset PVA$^-$ of a blocked regime was inherited from the block of the preceding regime. Focusing specifically on blocked-to-blocked regime transitions (40.2 % of all cases), for each time step of an active blocked regime, we identified the PVA$^-$ with the largest overlap with the regime mask as the 'dominant' PVA$^-$. If the onset PVA$^-$ of a blocked-to-blocked transition coincided with the dominant PVA$^-$ of the preceding regime, the two regimes could be connected. We find that 57 % of blocked regime onsets are linked to the dominant PVA$^-$ from the previous block, whenever the onset follows a blocked regime. This indicates that PVAs$^-$ do not necessarily form independently of the previous blocked regime but are instead displaced or reorganized remnants of the earlier blocking configuration. Along the retrogression pathway, notable continuity was found for transitions from ScBL to GL (60 %), EuBL to AR (76 %), and AR to GL (92 %). For the upstream pathway, strong linkages of PVA$^-$ were observed for EuBL-to-ScBL (77 %) and AR-to-EuBL (88 %) transitions. However, not all transitions exhibit such continuity. During GL-to-ScBL transitions, the PVA$^-$ dominating the onset is unconnected to the preceding GL block in 72 % of cases, which implies that the ScBL block forms in situ rather than as a continuation of the GL anomaly.

https://doi.org/10.5194/egusphere-2025-6306
Preprint. Discussion started: 28 December 2025

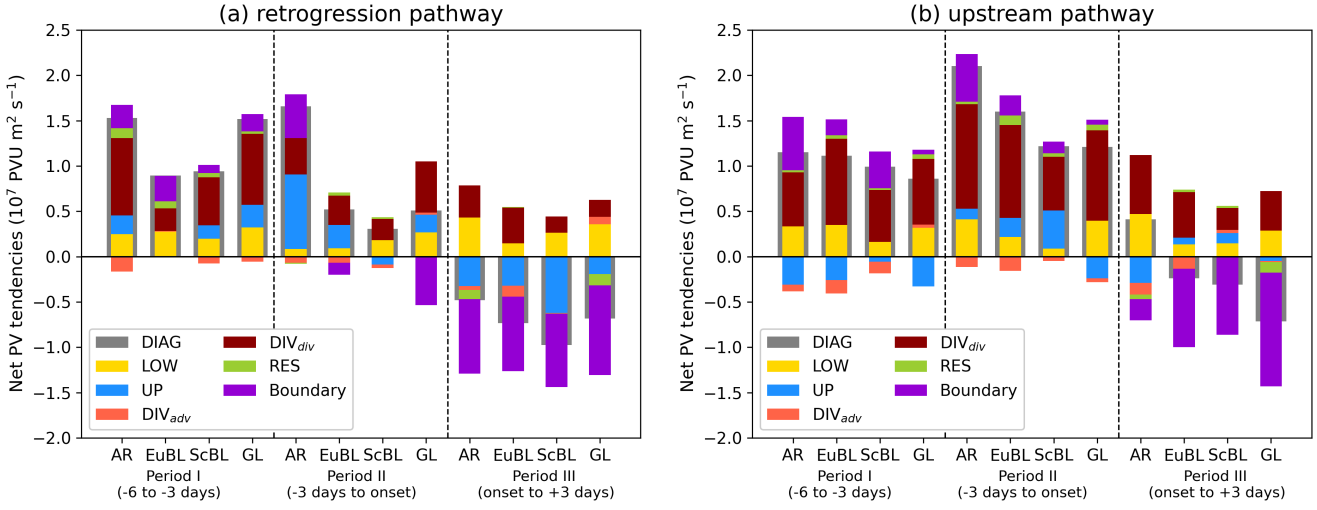

Figure 7. Net effect of amplitude evolution (grey bar) and contributing processes (coloured bars, see legend) for three different time periods (I, II and III; see x-axis for exact time lag information) and the four blocked regimes, split up into the onset PVAs$^-$ following the (a) retrogression and (b) upstream pathway.

3.3 The role of dry and moist processes for amplitude evolution

In this section, we first take a regime-centred perspective and consider the amplitude evolution of onset PVAs$^-$ relative to regime onset, consistent with previous studies of weather regime dynamics (e.g., Teubler et al., 2023). Subsequently, we switch to an anomaly-centred perspective and consider the evolution relative to the maximum amplitude of onset PVAs$^-$.

3.3.1 Regime-centred perspective

We start by examining the amplitude evolution of onset PVAs$^-$, irrespective of regime type or pathway (Figure 6a). From this broad perspective, onset PVAs$^-$ amplify on average in the days before blocked regime onset, with a peak 1-2 days before onset (DIAG, black line). Onset PVAs$^-$ still amplify during and after onset, reaching their peak amplitude around 1 day after the onset which is then followed by a weakening afterwards. This result highlights that onset PVAs$^-$ not only form remotely but also experience much of their amplification before the actual blocked regime onset. The divergent PV tendency (DIV$_{div}$, dark red) leads the total diagnosed amplification before the onset, pointing to a dominant contribution of moist processes for the build-up of the PVA$^-$ linked to blocked regime onset. After onset, the contribution of DIV$_{div}$ weakens but still brings a positive contribution the the amplitude evolution. The baroclinic interaction term (LOW, gold) shows a quite constant and positive contribution to the amplification of onset PVAs$^-$, which increases even further after onset probably as a result of coupling between the lower and upper troposphere. Upper-tropospheric, quasi-barotropic wave dynamics (UP, blue) provide the second most important contribution to a PVA$^-$ strengthening within the period -3 to +1 day around the onset and then a weakening beyond that. The impact of the divergent PV tendency due to the advection of background PV by the divergent wind

https://doi.org/10.5194/egusphere-2025-6306
Preprint. Discussion started: 28 December 2025

(DIV$_{adv}$, light red) and the residual PV tendency term (RES, yellow green) are negligibly small and not of any importance for the mean amplitude evolution.

The full boundary term (Boundary, dark violet) shows a positive contribution until about one day before onset, followed by a rapid and strong negative contribution that dominates the amplitude weakening afterward. When separated into its components (cf. Equation 3), the two contributions act in opposite directions before onset (not shown). The eddy PV flux term continuously weakens the onset PVA$^-$ amplitude, indicating a net inward PV flux across the anomaly boundary. In contrast, the area-change term suggests spatial growth or merging of smaller anomalies before onset, contributing to amplification. This aligns with the observed increase in anomaly area (grey line, Figure 6a). After onset, the full boundary term becomes negative as shrinking or splitting PVAs$^-$ reduce amplitude. Notably, this sign reversal occurs before the PVAs$^-$ reach their maximum size.

Considering the blocked regime types individually (Figure 6b), we find that for all types the onset PVAs$^-$ amplify in the days before onset and then start to weaken in the first two days after regime onset. One difference among the regimes is the rate of onset PVA$^-$ amplification. Low-latitude regimes (AR, EuBL) tend to amplify more than high-latitude regimes (ScBL, GL), which may partly reflect their larger initial size (not shown). A clear difference between the types, however, is found in the timing of the maximum amplification rate: EuBL and AR reach a peak in the two days before onset, ScBL peaks earlier, and GL shows a relatively flat amplification without a distinct maximum.

We further stratify by pathway and, given the differences in maximum amplification timing, we analyse two periods: -6 to -3 days (period I) and -3 days to onset (period II; see vertical dashed line in Figure 6b). Figure 7 provides a compact view on the net effect of the amplitude change of onset PVAs$^-$ and the respective PV tendency terms, allowing for a concise view of PV dynamics across regime types, timings, and pathways. First, we find differences in the timing of maximum amplification rate of onset PVAs$^-$ depending on the regime type and the pathway. Retrograding PVAs$^-$ intensify most during the earlier window, whereas in the final three days before onset their amplification is weaker—or comparable, in AR—relative to period I. By contrast, PVAs$^-$ following the upstream pathway show their strongest amplification in the latter period (Figure 7).

Second, we find pathway-specific differences in the contributions of dry and moist processes to the onset PVA$^-$ amplification and weakening rates. DIV$_{div}$ is the the major contribution to the amplification rate of onset PVAs$^-$ following the upstream pathway (Figure 7b). Because of its dominant role in the amplification of onset PVAs$^-$, we dedicate a chapter that provides more insights into the patterns and dynamics of DIV$_{div}$ (Section 3.4). The contribution of LOW is throughout positive, independent of pathway, time period relative to onset or blocked regime type. Thereby the magnitude of the net LOW contribution is highest for GL in both time periods before onset. For ScBL, the net effect of LOW is much lower compared to the other regimes and suggests less coupling with lower troposphere dynamics, probably linked to the location of the onset PVAs$^-$ in higher latitudes and over the continent. This agrees with the weaker tendencies of LOW in a spatial sense for onset PVAs$^-$ of ScBL (Figure 8d,h).

The sign of the net contribution of UP strongly depends on the pathway, blocked regime type and the timing. UP has an amplifying effect on onset PVAs$^-$ following the retrogression pathway in early times while those following the upstream pathway experience weakening via the UP term (Figure 7). A better agreement exists between the pathways shortly before onset, with UP leading to a net contribution to amplification as the quasi-barotropic tendency pattern enhances the western

https://doi.org/10.5194/egusphere-2025-6306
Preprint. Discussion started: 28 December 2025

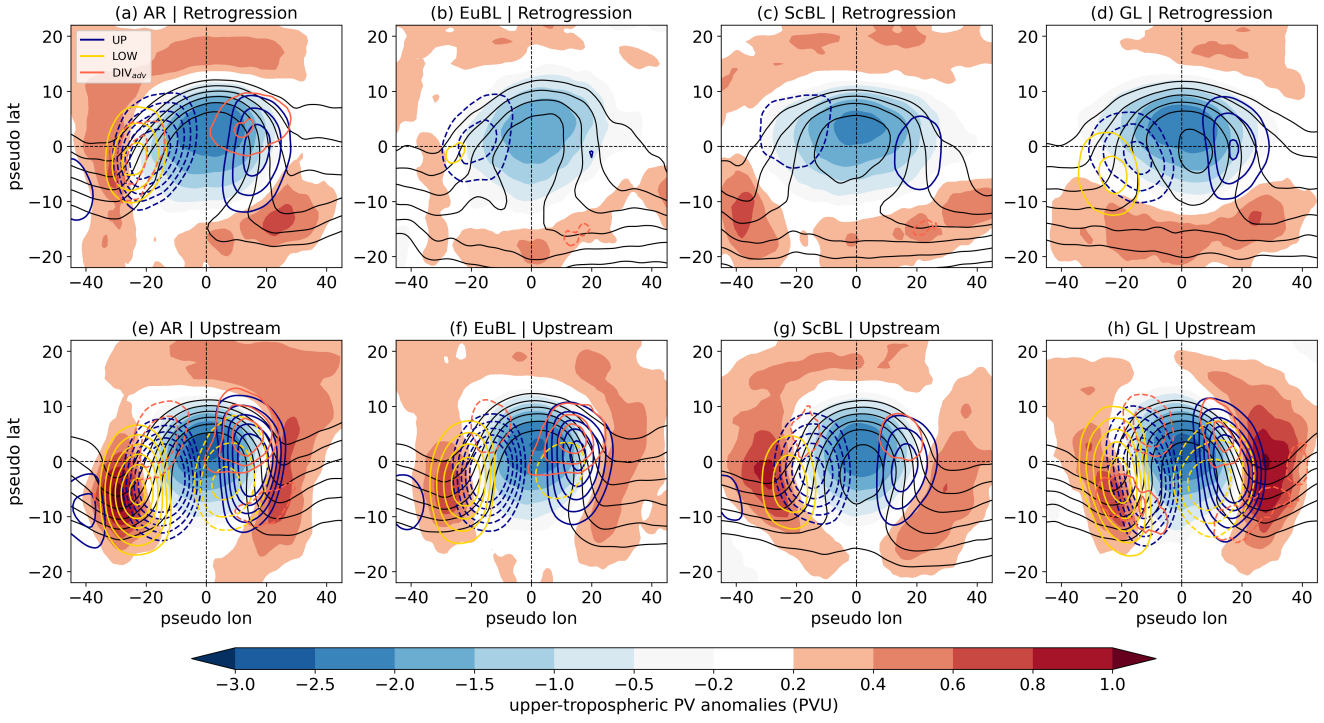

Figure 8. Centred composites on onset PVAs$^-$ (centre of mass positions) for the time period -3 days before onset to onset for the four blocked regimes (columns) and the two pathways (rows). Shading shows upper-tropospheric PV anomalies (in PVU, note the differences in colorbar extent) and black contours show the absolute PV in the upper troposphere (for the levels 2.5 to 5 PVU in steps of 0.5 PVU). Blue contour lines mark the contribution of UP (in steps of +/- 10, 14, 18, 22, 26 $\cdot$ 10^7 PVU m^2 s^{-1}), gold contour lines mark the contribution of LOW (in steps of +/- 1.2, 1.6, 2, 2.4, 2.8, 3.2 $\cdot$ 10^7 PVU m^2 s^{-1}) and light red contour point to tendencies of DIV$_{adv}$ (in steps of +/- 0.8, 1.2, 1.6, 2 $\cdot$ 10^7 PVU m^2 s^{-1}). Solid and dashed contours show positive and negative PV tendencies, respectively. In contrast to the area-integrated perspective (e.g., Figure 6a), negative (dashed) values here represent PV reduction, enhancing the PVAs$^-$, whereas positive (solid) values represent PV increase, weakening the PVAs$^-$.

flank more strongly than it suppresses the eastern flank (Figure 8). The boundary term contributes mostly positively to the amplitude evolution before the onset, and strongly negative after onset (Figure 7). However, for GL, the onset PVA$^-$ following the retrogression pathway experience a weakening by the boundary term before onset, which can probably be explained by an amplification that is re-strengthening an existing onset PVA$^-$, but without necessarily increasing its size, but making it more compact. The net effects of DIV$_{adv}$ and RES are of minor importance and are not further discussed here.

Third, onset PVAs$^-$ exhibit striking differences in their spatial characteristics depending on the pathway and the blocked regime type (Figure 8). The onset PVAs$^-$ following the upstream pathway have pronounced troughs upstream and downstream, which indicates that these anomalies are embedded within a RWP (Figure 8, lower row). This is not evident for retrograding onset PVAs$^-$ (Figure 8, upper row). Rather, the meridional orientation of PV anomalies indicate wave breaking, which often

https://doi.org/10.5194/egusphere-2025-6306
Preprint. Discussion started: 28 December 2025

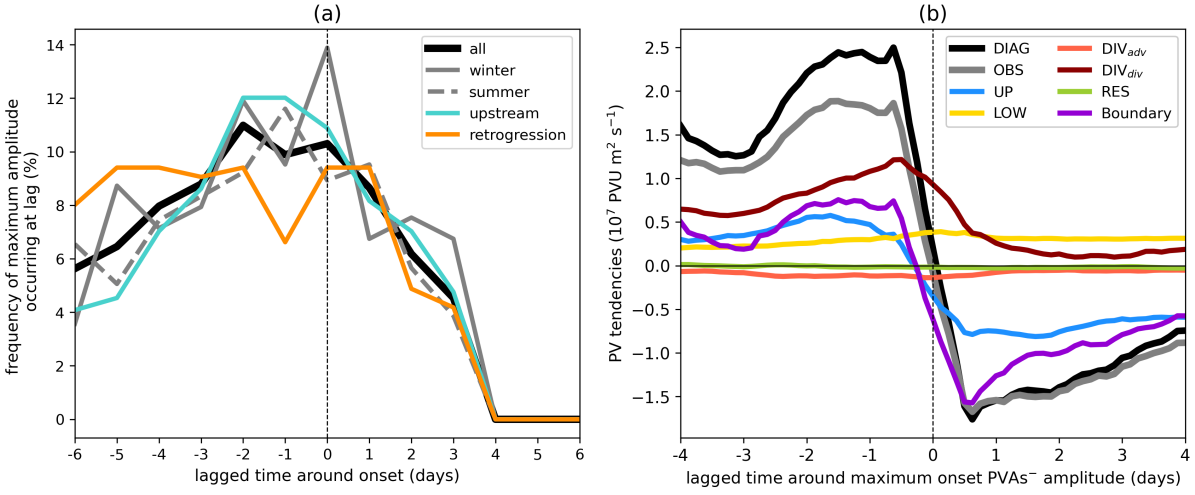

Figure 9. (a) Timing of maximum amplitude for onset PVAs$^-$ within the period -6 to +6 days around onset for all year-round regime life cycles (black), only for those in extended winter (NDJFM, solid grey) and extended summer (MJJAS, dashed grey), for all following the upstream pathway (turquoise) and the retrogression pathway (orange). (b) Mean of integrated PV tendencies over the onset PVAs$^-$ centred on the timing of their maximum amplitude (see panel a) and for all blocked regime life cycles. The lines have been smoothed by performing a centred 24 h running-mean.

occurs at the end of a RWP life cycle (Wirth et al., 2018). Previous studies show that peak frequencies of RWP initiation and decay are found at the beginning and the end of the North Atlantic storm track (Quinting and Vitart, 2019). PVAs$^-$ following the upstream pathway to ScBL onset are situated in regions where RWPs typically decay (Figure 4c). This positioning often results in the upstream trough exhibiting greater amplitude, which in turn leads to a quasi-barotropic enhancement of the onset PVAs$^-$ along their western flank (Figure 8h). In contrast, the onset PVAs$^-$ associated with GL propagate from upstream regions through areas where RWPs are typically initiated and therefore represent the trailing edge of an RWP, which is evident by a stronger trough downstream of the onset PVAs$^-$ (Figure 8e).

Taken together, these results show that onset PVAs$^-$ undergo substantial pre-onset amplification through a combination of moist divergence, baroclinic growth, and quasi-barotropic wave dynamics, with the relative contributions depending strongly on both regime type and pathway.

3.3.2 Anomaly-centred perspective

The onset-centred perspective revealed a systematic difference in the mean timing of maximum amplification of onset PVAs$^-$ between blocked regimes and pathways. However, differences in the timing within the individual pathways raise the question of whether the PVAs$^-$ involved in blocked regimes differ in their life cycles.

More than 80 % of all onset PVAs$^-$ attain their maximum amplitude before or at the time of onset, with the overall maximum occurring two days prior (Figure 9a). No clear seasonal signal is apparent, indicating that the timing is year-round consistent

https://doi.org/10.5194/egusphere-2025-6306
Preprint. Discussion started: 28 December 2025

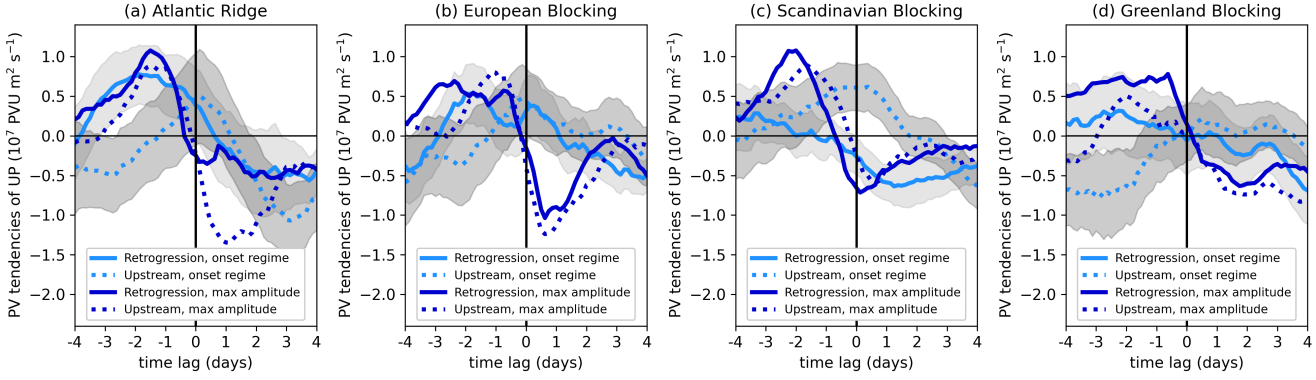

Figure 10. Temporal evolution of the upper-tropospheric PV tendency contribution to the amplitude change of onset PVAs$^-$ relative to the regime onset (light blue) and relative to the maximum in PVA$^-$ amplitude (dark blue) for the retrogression pathway (solid) and the upstream pathway (dotted). The x-axis shows the time lag around regime onset for the light blue lines and the time lag relative to the maximum amplitude of onset PVAs$^-$ for the dark blue lines. Grey shading displays +/- 1 standard deviations around the mean for the onset-centred perspective (light blue lines). The lines were smoothed using a 24 h moving window (+/- 12 h).

(grey lines). However, distinct differences emerge when the pathways are considered separately: Most onset PVAs$^-$ following the retrogression pathway reach their maximum in amplitude very early or shortly after onset (orange line), whereas those following the upstream pathway show a pronounced maximum in the two days before onset (turquoise line). This corresponds well with the findings above that retrograding onset PVAs$^-$ experience the strongest amplification between -6 to -3 days, while upstream PVAs$^-$ are primarily amplified shortly before onset (Figure 7).

A much clearer depiction of the amplification of onset PVAs$^-$ arises when examining the evolution of the amplitude tendency and the associated PV tendency terms from a perspective centred on the life cycle of each onset PVA$^-$, rather than relative to blocked regime onset (Figure 9b). By design, the amplitude increases and decreases before and after the maximum (lag 0), respectively. In agreement with the onset-centred perspective (Figure 6a), the dominant contribution to onset PVA$^-$ amplification is governed by DIV$_{div}$ and it exhibits a peak in the day before the maximum amplitude is reached. The contribution strongly decreases within the two days around the maximum, pointing to a lack of moist processes that could further amplify the onset PVA$^-$. LOW shows an increasing contribution to amplification during the life cycle of onset PVAs$^-$ compared to the evolution from the onset-centred perspective (Figure 9b), which indicates a rather constant contribution. The boundary term follows qualitatively the full amplification rate and points to an increase in the size of the PVA$^-$ before and a decrease after the maximum. However, the most distinct change is visible in the evolution of UP when comparing the onset-centred and the amplitude-centred perspective (Figure 6a vs. Figure 9b).

To further explore these differences in UP between the two perspectives, Figure 10 shows the mean evolution of UP for all blocked regimes and their corresponding two pathways, relative to regime onset and amplitude maximum of the onset PVA$^-$. In agreement with the compact view on net PV tendencies (cf. Figure 8), the contribution of UP relative to regime onset highly differs between the pathways and regimes (Figure 10, light blue), with partly opposite behaviour, such as for the two pathways

https://doi.org/10.5194/egusphere-2025-6306
Preprint. Discussion started: 28 December 2025

of ScBL and GL. Thereby, the mean evolution features multiple instances where the sign of UP changes. In contrast, a much clearer pattern emerges for UP in the anomaly-centred perspective (dark blue), with markedly smaller differences between pathways and regimes. The UP evolution across the different pathways and regimes largely follows the mean over all regimes and pathways (Figure 9b), with a positive contribution to amplification before the maximum amplitude and a contribution to weakening after. This indicates that the amplitude-centred framework captures an essential role of UP in the growth and decay of onset PVAs$^-$, while the onset-centred view highlights pathway-specific variability in the underlying dynamics.

3.4 The importance of moist processes and the link to WCB activity

A major result of this study is the dominance of moist processes during the amplification phase of onset PVA$^-$s prior to blocked regime onsets, as presented in Section 3.3. Here, we investigate the spatial distribution of amplifying DIV$_{div}$ tendencies and WCB activity within the onset PVA$^-$s, and analyse whether the contribution of moist processes depends on the geographic position of the PVA$^-$s relative to the storm track. Given the maximum in DIV$_{div}$ during the two days preceding blocked regime onsets (cf. Figure 6a) and to be consistent with Figure 8, we present onset PVA$^-$-centred composites of WCB activity and DIV$_{div}$ tendencies for the period from -3 days to onset (corresponding to period II in Figure 7), shown separately for the four blocked regimes and pathways.

Onset PVAs$^-$ of most regimes and pathways reveal amplifying DIV$_{div}$ tendencies to the northwest of the PVA$^-$ centre, with a distinct WCB structure before regime onset: WCB inflow in the southwestern, WCB ascent in the western, and WCB outflow in the northern part of the anomaly (Figure 11). This composite structure of the full WCB corresponds well with many case study-based findings of WCB activity along the western edge of a ridge or block (e.g., Grams et al., 2011). There is a strong spatial overlap of WCB outflow, negative DIV$_{div}$ tendencies, and areas of pronounced upper-tropospheric divergence (wind vectors in Figure 11), all located to the northwestern part of the anomaly. Consistent with this spatial linkage, we find a modest, significant positive correlation between the anomaly-integrated DIV$_{div}$ tendencies and WCB area size within the onset PVAs$^-$, with r = 0.32 for WCB ascent and r = 0.34 for WCB outflow. Hauser et al. (2023) demonstrated this relationship for a single case, but here we show that the relationship holds systematically in a climatological sense, i.e., in the average over many cases. This result confirms the notion that tropopause modification by upper-tropospheric divergent flow is enhanced by latent heat release in WCBs and establishes a direct link between WCBs and the divergent PV tendencies that reinforce negative PV anomalies. Upper-level convergence, in contrast, occurs in the eastern part of the onset PVAs$^-$, where it contributes to a local increase in PV. However, when considered in an integrated sense, the anomaly-amplifying tendencies of DIV$_{div}$ dominate, resulting in a net amplifying effect of DIV$_{div}$ (cf. Figure 7).

High variations are found in the activity and co-occurrence of WCBs with onset PVAs$^-$ before onset, showing a strong dependency on the blocked regime type and, in particular, on the pathway (Figure 11). More frequent WCB activity and stronger amplifying DIV$_{div}$ tendencies occur for onset PVAs$^-$ following the upstream pathway (Figure 11, upper vs. lower panels). The strongest WCB activity is observed for onset PVAs$^-$ that follow the upstream pathway of AR, EuBL, and GL, and is characterized by a high outflow frequency covering the northern half of the onset PVAs$^-$. In contrast, WCB activity is much weaker for PVAs$^-$ following the upstream pathway of ScBL and for those following the retrogression pathway of AR and

https://doi.org/10.5194/egusphere-2025-6306
Preprint. Discussion started: 28 December 2025

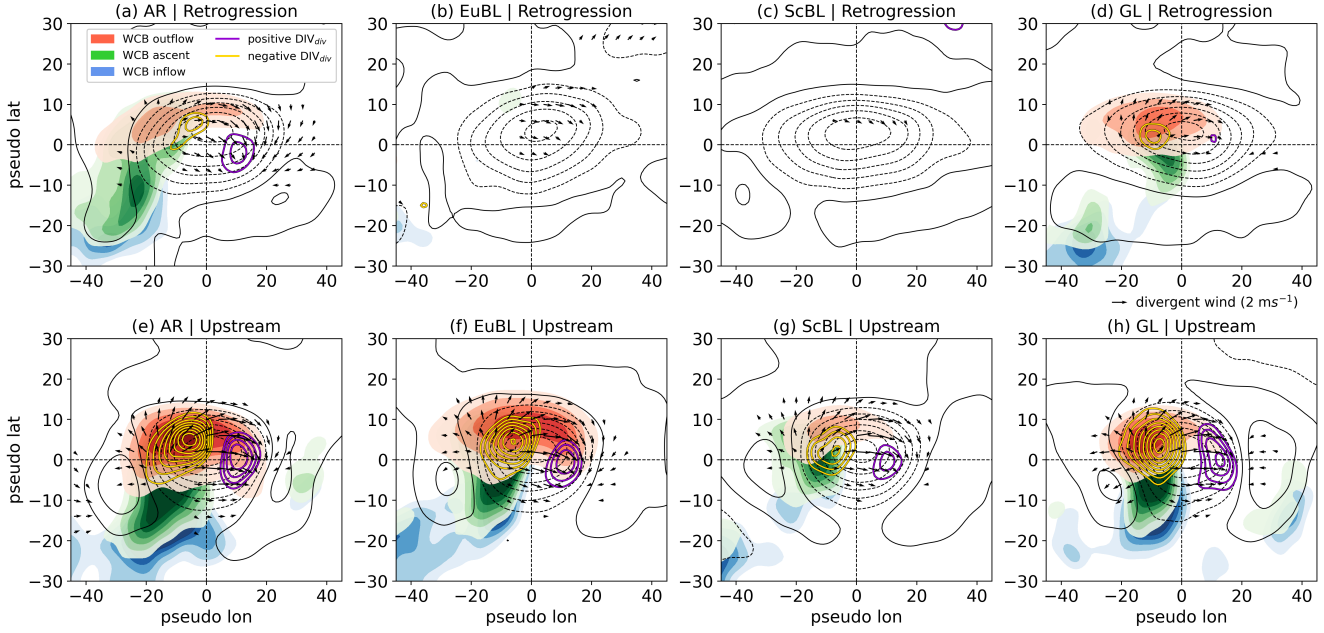

Figure 11. Centred composites of onset PVAs$^-$ (centre of mass positions) for the time period -3 days to onset for the four blocked regimes (columns) and the two pathways (rows). Solid and dashed black lines show positive and negative upper-tropospheric PV anomalies, respectively (+/- 0.2, 0.6, 1.0, 1.4, 1.8, 2.2, 2.6 PVU). Shading in different colours point to WCB frequencies for WCB inflow (blue; 2, 2.5, 3, 3.5, 4 %), WCB ascent (green; 2, 2.5, 3, 3.5, 4, 4.5 %) and WCB outflow (red; 6, 8, 10, 12, 14, 16 %). Gold (dark violet) solid contours mark negative (positive) tendencies of DIV$_{div}$ (from +/- 0.3 to +/- 1.0 $\cdot$ 10^7 PVU m^2 s^{-1} in steps of 0.1). Wind vectors (in black) show the divergent wind speed and direction whenever the wind speed exceeds 0.7 m s^{-1}. All field were smoothed by a Gaussian filter with σ = 2.

GL. Most notably, onset PVAs$^-$ following the retrogression pathways of EuBL and ScBL do not exhibit strong WCB activity, which is in stark contrast to the onset PVAs$^-$ following the upstream pathway within the same regimes. While DIV$_{div}$ makes a substantial net contribution to the PVA$^-$ amplification along the retrogression pathway (Figure 7a), the signal is weak in the mean spatial composites (Figure 11b,c). This is likely due to several factors, such as changes in anomaly size and shape that smear the signal and maybe even contributions from processes that are not related to WCBs.

As argued for GL (Hauser et al., 2024b), upstream WCB activity may further enhance retrogression and maintain onset PVAs$^-$ on the upstream flank. Generalized for all blocked regimes, the upstream WCB activity and DIV$_{div}$-related amplification on the western flank are weaker for retrograding PVAs$^-$ compared to PVAs$^-$ following the upstream pathway (Figure 11, upper row vs. lower row). Moist processes aid anomaly retrogression by extending and strengthening PVAs$^-$ westward, leading to a reduced propagation of ridges (e.g., Riemer et al., 2014). Hence, the observed westward propagation of onset PVAs$^-$ is likely supported by moist, rather than dry, dynamics alone. Although upstream WCB activity and DIV$_{div}$-related amplification on the western flank are weaker for retrograding PVAs$^-$ (Figure 11, upper row), they suggest that moist processes aid anomaly retrogression by extending and strengthening PVAs$^-$ westward, as noted in Hauser et al. (2024b).

https://doi.org/10.5194/egusphere-2025-6306
Preprint. Discussion started: 28 December 2025

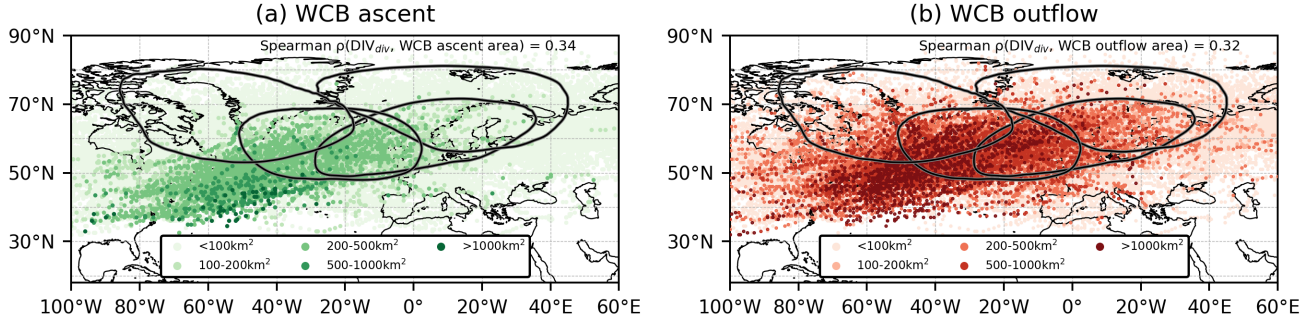

Figure 12. Scatter plot showing the position (centre of mass) and the area of (a) WCB ascent and (b) WCB outflow within the onset PVA$^-$ for the time period -6 days to +3 days around blocked regime onset, independent of pathway, season or blocked regime type. The black contours mark the regime masks for the four blocked regimes (cf. Figure 2). The Spearman correlation between the strength of DIV$_{div}$ tendencies and the area of WCB ascent/outflow is displayed in the figures and both values are statistically significant (p-value < 0.05).

The partly large differences in WCB activity between the blocked regime types and pathways raise the question of whether the location of onset PVAs$^-$ is crucial for the role of moist processes in amplifying onset PVAs$^-$. Figure 12 shows that PVAs$^-$ located over the midlatitude storm-track regions of the North Atlantic exhibit a much larger area of WCB activity within the PVA$^-$ area compared with those elsewhere, revealing that the location of onset PVAs$^-$ indeed matters. Differences between the distributions of WCB ascent and outflow in Figure 12 can largely be explained by the facts that the WCB ascent area is much smaller than the WCB outflow area, and their climatological occurrences differ, with WCB ascent often concentrated over the western and central North Atlantic, while WCB outflow is more broadly spread across the entire North Atlantic domain (e.g. Heitmann et al., 2024).

To conclude, the close link between WCB activity and amplifying DIV$_{div}$ tendencies (cf. Figure 11) underscore the importance of moist processes along the pathways of onset PVAs$^-$. Onset PVAs$^-$ crossing the North Atlantic storm-track region are more likely to be amplified by moist processes than those propagating through more continental areas (Figure 12), such as the retrogression pathways of EuBL and ScBL.

4 Summary and concluding discussion

In this study, we examined the onset dynamics for four blocked weather regimes over the North Atlantic–European region, using ERA5 reanalysis data for 1979–2021. Building on the quasi-Lagrangian potential vorticity (PV) framework introduced by Hauser et al. (2023), we traced negative upper-tropospheric PV anomalies (onset PVAs$^-$) associated with blocked regime onset and diagnosed the relative contributions of dry-dynamical and moist-dynamical processes to the amplitude evolution of onset PVAs$^-$.

https://doi.org/10.5194/egusphere-2025-6306
Preprint. Discussion started: 28 December 2025

To place these results in context, the following subsections summarize the main findings of this study in response to the research questions raised in the introduction and situate them within the existing literature. We conclude by discussing the broader relevance and implications of our results and outlining key limitations and directions for future research.

4.1 The non-local development of onset PVAs$^-$

Considering 729 blocked regime life cycles over the North Atlantic-European region, this study provides a quasi-Lagrangian view on the origin and propagation of onset PVAs$^-$. These anomalies do *not* develop in-situ but rather propagate into the target region within the blocked regime pattern. Based on their location in the days before blocked regime onset, most onset PVAs$^-$ approach their blocked regime location from upstream, i.e., from the west of or within the North Atlantic–European sector, consistent with previous findings that identify the western North Atlantic as a typical genesis region for atmospheric blocks (Croci-Maspoli et al., 2007; Steinfeld and Pfahl, 2019). For EuBL, more than 75 % of onset PVA$^-$s follow the upstream pathway, supporting earlier results linking European blocking to Rossby wave trains from the subtropical western Atlantic (Michel and Rivière, 2011; Drouard et al., 2021).

Retrogression of blocks has received less attention, although early work (Sumner, 1954; Lejenäs, 1983) already highlighted this behaviour, particularly in spring. GL is the only blocked regime with a consistently more frequent retrogression pathway (58 %) than an upstream one. Previous studies have suggested that processes on the western flank of a block can lead to westward expansion or displacement (Steinfeld and Pfahl, 2019), and that divergent outflow may decelerate the eastward propagation of ridges or blocks (Riemer and Jones, 2014). In agreement with Hauser et al. (2024b), we show that amplification by moist processes on the western flank likely contributes, alongside barotropic dynamics, to the westward propagation of PVA$^-$s before blocking onset. When viewed alongside Steinfeld et al. (2020) and Deshmukh et al. (2025), these results suggest that moisture can modulate block retrogression, as dry simulations typically exhibit a more zonal flow and less pronounced westward displacement.

Propagation of blocks has also been studied in the context of weather regime transitions (e.g., Vautard, 1990; Michel and Rivière, 2011; Ferranti et al., 2015). Vautard (1990) linked the propagation and dissipation of blocking highs to regime transitions over the North Atlantic–European region. We find that a single PVA$^-$ can contribute to multiple blocked regimes during such transitions, explained by overlapping pathways and formation regions between successive regimes. The AR–GL transition, characterized by northwestward-propagating PVA$^-$s from the central North Atlantic, was already described by Vautard (1990). Using our quasi-Lagrangian PV perspective, we confirm that 92 % of AR–GL transitions involve retrogression of the PVA$^-$ from the eastern North Atlantic toward Greenland. Likewise, the upstream propagation of anticyclones associated with EuBL–AR transitions (Büeler et al., 2021) is confirmed in 76 % of cases where onset PVAs$^-$s of AR followed the retrogression pathway.

4.2 Role of dry and moist dynamics for onset PVAs$^-$

Using the quasi-Lagrangian PV framework, we reveal that onset PVAs$^-$ strong amplify in the days before the actual blocked regime onset, independent of pathway and blocked regime type. Thereby, the amplitude evolution shows greater similarity

https://doi.org/10.5194/egusphere-2025-6306
Preprint. Discussion started: 28 December 2025

across all blocked regimes than between the two pathways: The timing of maximum amplification poses the major disparity with a later amplification of upstream PVAs$^-$ and a much earlier amplification of retrograding PVAs$^-$. Anomaly-amplifying divergent PV tendencies (DIV$_{div}$) contribute dominantly to this amplification and we confirm their link to latent heat release in WCBs. Previous climatological studies have highlighted the importance of moist contributions to blocking onset (e.g., Pfahl et al., 2015; Steinfeld and Pfahl, 2019), using a purely Lagrangian perspective based on air-parcel trajectory diagnostics. Baroclinic interaction and the general growth in PVA$^-$ area are of secondary importance and further strengthen the PVA$^-$ amplitude. The role of quasi-barotropic wave dynamics depends on the pathway and shows sometimes a contribution to the weakening, sometimes to the strengthening of a PVA$^-$.

A closer look at the DIV$_{div}$-WCB activity link revealed that the contribution of moist processes depends on the location of onset PVAs$^-$ relative to the storm-track region—consistent with Steinfeld and Pfahl (2019), who reported stronger latent-heating effects for Atlantic than for continental blocks. Overall, the moist contribution is stronger for the upstream pathway, as these onset PVAs$^-$ typically reside within or near the midlatitude storm track where WCB activity is frequent. For the retrogression pathway, moist processes can still support the amplification and westward extension of onset PVAs$^-$ when they intersect the storm-track region over the North Atlantic during their westward propagation. Our results also align with Steinfeld and Pfahl (2019) regarding the timing of moist amplification. They showed that extending backward trajectories from 3 to 7 days substantially increases the share of heated trajectories, indicating that moist processes can act well before blocking onset. This timing dependence is consistent with our finding that moist amplification occurs earlier for retrogressing onset PVAs$^-$, whereas upstream PVAs$^-$ intensify closer to the onset. Extending the analysis period therefore captures the moisture contribution of all PVAs$^-$, including those that experienced earlier, weaker amplification phases.

Using an anomaly-centred perspective, a clearer picture emerged on the life cycle dynamics of onset PVAs$^-$ for different blocked regimes and pathways. Divergent PV tendencies still dominate the amplification, but the contribution of quasi-barotropic wave dynamics is more distinct and consistently acts to strengthen the PVA$^-$, in comparison to the onset-centred perspective. This indicates that the relative importance of quasi-barotropic dynamics (UP) is highly sensitive to the choice of time reference—whether aligned with the blocked regime onset or with the PVAs$^-$ maximum amplitude. Comparing the evolution of onset PVAs$^-$ to the amplitude evolution of negative PV anomalies linked to ridges as part of RWPs (Teubler and Riemer, 2016, 2021) highlights that the processes governing the amplification are quite similar: Onset PVAs$^-$ grow by downstream development (UP), the peak of which is followed by a growth in LOW and, in particular DIV$_{div}$ - a process chain referred to as downstream moist-baroclinic development (Orlanski and Sheldon, 1995; Teubler and Riemer, 2021).

The fact that the maximum amplitude of onset PVAs$^-$ does not coincide with the blocked regime onset implies that the onset of blocked regimes is governed less by the in-situ amplification of individual anomalies and more by the reorganization of pre-existing PVAs$^-$ into the large-scale blocked pattern. This finding stems from how blocking is defined in our study through the lens of weather regimes. While specific blocking indices often depend on the intensity of a block (e.g., Schwierz et al., 2004; Pinheiro et al., 2019), the weather regime perspective emphasizes the similarity of the large-scale circulation pattern, with a secondary importance on the pattern's strength. This allows for more transience, such that the onset of a blocked regime does not necessarily coincide with a peak in the intensity of the respective PVA$^-$. Moreover, the PVA$^-$ triggering the onset of a

https://doi.org/10.5194/egusphere-2025-6306
Preprint. Discussion started: 28 December 2025

blocked regime is not always the same as the one dominating at the regime maximum (cf. Hauser et al., 2024b, their Figure 9a), underscoring the role of transient eddies in shaping the blocking structure (Suitters et al., 2023). Together, these results highlight that the transition to a blocked regime reflects a structural reconfiguration of the flow rather than the continued local growth of a single PV anomaly.

4.3 Comparison with Eulerian perspective on blocked regime dynamics

Teubler et al. (2023) analysed the same types of blocked regimes during the same time period as in the current study from an Eulerian PV perspective. In that study, very similar PV tendency terms were projected onto the regime patterns to assess the relative importance of different processes in building the regime pattern. In contrast to our focus on the negative PV anomaly, the results published in Teubler et al. (2023) pertain to the full regime pattern, including the area of the patterns' positive PV anomaly. When computing the projections only for the region of the positive and negative PV anomaly, respectively, the results look very similar on average, as documented for a single case in Hauser et al. (2023).

For all blocked regime life types, Teubler et al. (2023) found that linear quasi-barotropic dynamics and non-linear eddy flux convergence dominate the regime development, while baroclinic and divergent PV tendencies contribute only marginally. That study also identified two clusters resembling the pathways found here. For any of the combinations of regime type and pathway, however, the influence of moist processes was found to be subordinate—contrasting with our results, which reveal a strong moist contribution when viewed from a different perspective.

Building on Hauser et al. (2023), who reconciled results from Eulerian, Lagrangian, and quasi-Lagrangian perspectives for a single case study, we here generalize these findings across the full life cycles of multiple blocked-regime types in the North Atlantic–European region and reconcile conclusions from previous Eulerian- and Lagrangian-based studies on blocking dynamics. The Eulerian perspective emphasizes the reorganisation of anomalies within the regime mask, rather than their initial amplification, highlighting a key distinction from the quasi-Lagrangian approach. Onset PVAs$^-$ mostly amplify in the days before blocked regime onset, when they are located outside of the regime mask. Hence their moist-dynamical contributions occurs remotely and the Eulerian perspective largely misses this formation and amplification stage, and instead captures the propagation of onset PVAs$^-$ into the regime mask as a form of anomaly reorganization within the dominant barotropic PV tendency term. Thus, the Eulerian signature of anomaly reorganisation is reconciled with the quasi-Lagrangian evidence of remote moist-driven PVA$^-$ amplification.

4.4 Relevance, limitations and future work

In conclusion, our quasi-Lagrangian PV analysis revealed two distinct PVA$^-$ onset pathways to blocked regimes, showing that pathway-dependent dynamics exceed differences between regime types, and underscoring the importance of moist processes in their amplification. These results reconcile previous inconsistencies regarding the roles of dry and moist processes, showing that both are essential but act at different stages and locations. By linking remote moist amplification of PVAs$^-$ with local dry, barotropic pattern formation, we gain a more unified understanding of how different blocked regimes and pathways emerge. The analyses using the quasi-Lagrangian PV framework also highlight the importance of capturing dry and moist processes

https://doi.org/10.5194/egusphere-2025-6306
Preprint. Discussion started: 28 December 2025

in models, especially the interactions across scales and the role of moist-baroclinic eddies, to improve the prediction and conceptual understanding of blocked regimes.

While the quasi-Lagrangian PV approach provides novel insights into the evolution and amplification of $PVAs^-$ linked to blocked regime onsets, several limitations remain. The sample size of blocked regime life cycles becomes limited when separating blocked regime types and pathways, which may affect the robustness of detailed, pathway-specific conclusions and further stratification, e.g., to examine seasonal variability. Our diagnostic tracks only negative PV anomalies, whereas the Eulerian framework considers both positive and negative anomalies in a joint framework, making it difficult to compare in more detail the quasi-Lagrangian insights with the full-pattern Eulerian results. Finally, the study focuses on (pre-)onset dynamics and does not address the full blocked regime life cycle or the factors determining regime duration, which is important for understanding how initial anomaly development translates into the persistence and decay of blocked regimes.

Our findings clarify the individual, isolated roles of moist and dry dynamics, but a key open question is why only some diabatically enhanced, slowly propagating $PVAs^-$—whose amplification closely resembles ridge growth in RWPs and largely samples the climatological distribution of WCB activity—ultimately develop into blocked regimes. Recent work by Vishnupriya et al. (2025) finds little evidence that these $PVAs^-$ have systematically distinct moist characteristics, suggesting that the key question is not the moist processes themselves, but the conditions under which remotely amplified anomalies develop into a block. Thus, the central challenge for future research is to understand the coupling between remote moist-dynamical amplification and local dry anomaly rearrangement, and what factors determine whether this coupling leads to blocking.

Data availability. The data are referenced in Section 2. ERA5 data are freely available at https://doi.org/10.24381/cds.bd0915c6 (Hersbach et al., 2020). The dataset of tracked negative, upper-tropospheric PV anomalies for the time period 1979–2021 for the full Northern Hemisphere can be retrieved at https://publikationen.bibliothek.kit.edu/1000169838 (see Hauser et al., 2024a). The warm conveyor belt footprints dataset based on ERA5 reanalysis fields by Quinting et al. (2022) are freely available at https://gitlab.kit.edu/julian.quinting/elias-2.0. The weather regime data can be downloaded from Zenodo at https://doi.org/10.5281/zenodo.17080146. The codes and data from this study can be provided by the authors upon request.

Author contributions. The analyses for this study were performed by SH, who also prepared the first draft of the manuscript. FT provided the piecewise PV tendencies, and CMG contributed the year-round North Atlantic–European weather regime data based on ERA5. All co-authors provided guidance throughout the project and offered feedback on the manuscript.

Competing interests. MR and CMG are members of the editorial board of Weather and Climate Dynamics. The authors have no other competing interests to declare.

https://doi.org/10.5194/egusphere-2025-6306
Preprint. Discussion started: 28 December 2025

Acknowledgements. The research leading to these results has been done within the sub-project "Dynamics and predictability of blocked regimes in the Atlantic-European region (A8)" of the Transregional Collaborative Research Center SFB / TRR 165 “Waves to Weather” (www.wavestoweather.de) funded by the German Research Foundation (DFG). SH additionally acknowledges funding from the Swiss National Science Foundation (SNSF, project 228019). The contribution of CMG is funded by the Helmholtz Association as part of the Young Investigator Group "Sub-seasonal Predictability: Understanding the Role of Diabatic Outflow" (SPREADOUT, grant VH-NG-1243). The authors would like to thank the members of the "Large-Scale Dynamics and Predictability" research group at KIT for valuable discussions on this project.

https://doi.org/10.5194/egusphere-2025-6306
Preprint. Discussion started: 28 December 2025

References

Austin, J. F.: The blocking of middle latitude westerly winds by planetary waves, Quarterly Journal of the Royal Meteorological Society, 106, 327–350, https://doi.org/10.1002/qj.49710644807, 1980.

Büeler, D., Ferranti, L., Magnusson, L., Quinting, J. F., and Grams, C. M.: Year-round sub-seasonal forecast skill for Atlantic–European weather regimes, Quarterly Journal of the Royal Meteorological Society, 147, 4283–4309, https://doi.org/10.1002/qj.4178, 2021.

Chagnon, J. M., Gray, S. L., and Methven, J.: Diabatic processes modifying potential vorticity in a North Atlantic cyclone, Quarterly Journal of the Royal Meteorological Society, 139, 1270–1282, https://doi.org/10.1002/qj.2037, 2013.

Croci-Maspoli, M., Schwierz, C., and Davies, H. C.: A multifaceted climatology of atmospheric blocking and its recent linear trend, Journal of Climate, 20, 633–649, https://doi.org/10.1175/JCLI4029.1, 2007.

Davini, P. and D'Andrea, F.: Northern Hemisphere atmospheric blocking representation in global climate models: Twenty years of improvements?, Journal of Climate, 29, 8823 – 8840, https://doi.org/10.1175/JCLI-D-16-0242.1, 2016.

Davis, C. A.: Piecewise Potential Vorticity Inversion, Journal of the Atmospheric Sciences, 49, 1397–1411, https://doi.org/10.1175/1520-0469(1992)049<1397:PPVI>2.0.CO;2, 1992.

Davis, C. A. and Emanuel, K. A.: Potential Vorticity Diagnostics of Cyclogenesis, Monthly Weather Review, 119, 1929–1953, https://doi.org/10.1175/1520-0493(1991)119<1929:PVDOC>2.0.CO;2, 1991.

Dee, D. P., Uppala, S. M., Simmons, A. J., Berrisford, P., Poli, P., Kobayashi, S., Andrae, U., Balmaseda, M. A., Balsamo, G., Bauer, P., Bechtold, P., Beljaars, A. C. M., van de Berg, L., Bidlot, J., Bormann, N., Delsol, C., Dragani, R., Fuentes, M., Geer, A. J., Haimberger, L., Healy, S. B., Hersbach, H., Hólm, E. V., Isaksen, L., Kållberg, P., Köhler, M., Matricardi, M., McNally, A. P., Monge-Sanz, B. M., Morcrette, J.-J., Park, B.-K., Peubey, C., de Rosnay, P., Tavolato, C., Thépaut, J.-N., and Vitart, F.: The ERA-Interim reanalysis: Configuration and performance of the data assimilation system, Quarterly Journal of the Royal Meteorological Society, 137, 553–597, https://doi.org/10.1002/qj.828, 2011.

Deshmukh, V., Rivière, G., Fromang, S., and Saint-Lu, M.: How Does a Dry General Circulation Model Represent Atmospheric Blocking?, Journal of the Atmospheric Sciences, 82, 283 – 300, https://doi.org/10.1175/JAS-D-24-0048.1, 2025.

Dolores-Tesillos, E., Martius, O., and Quinting, J.: On the role of moist and dry processes for atmospheric blocking biases in the Euro-Atlantic region in CMIP6, EGUsphere, 2024, 1–25, https://doi.org/10.5194/egusphere-2024-2878, https://egusphere.copernicus.org/preprints/2024/egusphere-2024-2878/, 2024.

Drouard, M. and Woollings, T.: Contrasting Mechanisms of Summer Blocking Over Western Eurasia, Geophysical Research Letters, 45, 12,040–12,048, https://doi.org/https://doi.org/10.1029/2018GL079894, https://agupubs.onlinelibrary.wiley.com/doi/abs/10.1029/2018GL079894, 2018.

Drouard, M., Woollings, T., Sexton, D. M. H., and McSweeney, C. F.: Dynamical differences between short and long blocks in the Northern Hemisphere, Journal of Geophysical Research: Atmospheres, 126, e2020JD034 082, https://doi.org/10.1029/2020JD034082, 2021.

Duchon, C. E.: Lanczos Filtering in One and Two Dimensions, Journal of Applied Meteorology and Climatology, 18, 1016 – 1022, https://doi.org/10.1175/1520-0450(1979)018<1016:LFIOAT>2.0.CO;2, 1979.

Ertel, H.: Ein neuer hydrodynamischer Erhaltungssatz, Die Naturwissenschaften, 30, 543–544, https://doi.org/10.1007/BF01475602, 1942.

Faranda, D., Masato, G., Moloney, N., Sato, Y., Daviaud, F., Dubrulle, B., and Yiou, P.: The Switching between Zonal and Blocked Mid-Latitude Atmospheric Circulation: A Dynamical System Perspective, Climate Dynamics, 47, 1587–1599, https://doi.org/10.1007/s00382-015-2921-6, 2016.

https://doi.org/10.5194/egusphere-2025-6306
Preprint. Discussion started: 28 December 2025

Feldstein, S. B.: Fundamental mechanisms of the growth and decay of the PNA teleconnection pattern, Quarterly Journal of the Royal Meteorological Society, 128, 775–796, https://doi.org/https://doi.org/10.1256/0035900021643683, 2002.

Ferranti, L., Corti, S., and Janousek, M.: Flow-dependent verification of the ECMWF ensemble over the Euro-Atlantic sector, Quarterly Journal of the Royal Meteorological Society, 141, 916–924, https://doi.org/10.1002/qj.2411, 2015.

Grams, C. M., Wernli, H., Böttcher, M., Čampa, J., Corsmeier, U., Jones, S. C., Keller, J. H., Lenz, C.-J., and Wiegand, L.: The key role of diabatic processes in modifying the upper-tropospheric wave guide: a North Atlantic case-study, Quarterly Journal of the Royal Meteorological Society, 137, 2174–2193, https://doi.org/10.1002/qj.891, 2011.

Grams, C. M., Beerli, R., Pfenninger, S., Staffell, I., and Wernli, H.: Balancing Europe's wind power output through spatial deployment informed by weather regimes, Nature Clim Change, 7, 557–562, https://doi.org/10.1038/nclimate3338, 2017.

Grose, W. L. and Hoskins, B. J.: On the Influence of Orography on Large-Scale Atmospheric Flow, Journal of Atmospheric Sciences, 36, 223 – 234, https://doi.org/10.1175/1520-0469(1979)036<0223:OTIOOO>2.0.CO;2, 1979.

Hauser, S., Teubler, F., Riemer, M., Knippertz, P., and Grams, C. M.: Towards a holistic understanding of blocked regime dynamics through a combination of complementary diagnostic perspectives, Weather and Climate Dynamics, 4, 399–425, https://doi.org/10.5194/wcd-4-399-2023, 2023.

Hauser, S., Teubler, F., Riemer, M., Knippertz, P., and Grams, C. M.: Tracks of negative upper-tropospheric PV anomalies ($PVAs^{-}$) over the Northern Hemisphere in ERA5 reanalysis (1979-2021), https://doi.org/10.35097/nncxPGLAaaDgVKIW, 12.11.34; LK 01, 2024a.

Hauser, S., Teubler, F., Riemer, M., Knippertz, P., and Grams, C. M.: Life cycle dynamics of Greenland blocking from a potential vorticity perspective, Weather and Climate Dynamics, 5, 633–658, https://doi.org/10.5194/wcd-5-633-2024, https://wcd.copernicus.org/articles/5/633/2024/, 2024b.

Heitmann, K., Sprenger, M., Binder, H., Wernli, H., and Joos, H.: Warm conveyor belt characteristics and impacts along the life cycle of extratropical cyclones: case studies and climatological analysis based on ERA5, Weather and Climate Dynamics, 5, 537–557, https://doi.org/10.5194/wcd-5-537-2024, https://wcd.copernicus.org/articles/5/537/2024/, 2024.

Henderson, S. A., Maloney, E. D., and Barnes, E. A.: The influence of the Madden-Julian oscillation on Northern Hemisphere winter blocking, Journal of Climate, 29, 4597–4616, https://doi.org/10.1175/JCLI-D-15-0502.1, 2016.

Hersbach, H., Bell, B., Berrisford, P., Hirahara, S., Horányi, A., Muñoz-Sabater, J., Nicolas, J., Peubey, C., Radu, R., Schepers, D., Simmons, A., Soci, C., Abdalla, S., Abellan, X., Balsamo, G., Bechtold, P., Biavati, G., Bidlot, J., Bonavita, M., De Chiara, G., Dahlgren, P., Dee, D., Diamantakis, M., Dragani, R., Flemming, J., Forbes, R., Fuentes, M., Geer, A., Haimberger, L., Healy, S., Hogan, R. J., Hólm, E., Janisková, M., Keeley, S., Laloyaux, P., Lopez, P., Lupu, C., Radnoti, G., de Rosnay, P., Rozum, I., Vamborg, F., Villaume, S., and Thépaut, J.-N.: The ERA5 global reanalysis, Quarterly Journal of the Royal Meteorological Society, 146, 1999–2049, https://doi.org/10.1002/qj.3803, 2020.

Hochman, A., Messori, G., Quinting, J. F., Pinto, J. G., and Grams, C. M.: Do Atlantic-European Weather Regimes Physically Exist?, Geophysical Research Letters, 48, e2021GL095 574, https://doi.org/10.1029/2021GL095574, 2021.

Hoskins, B. J., McIntyre, M. E., and Robertson, A. W.: On the Use and Significance of Isentropic Potential Vorticity Maps, Quarterly Journal of the Royal Meteorological Society, 111, 877–946, https://doi.org/10.1002/qj.49711147002, 1985.

Kautz, L.-A., Martius, O., Pfahl, S., Pinto, J. G., Ramos, A. M., Sousa, P. M., and Woollings, T.: Atmospheric blocking and weather extremes over the Euro-Atlantic sector – a review, Weather and Climate Dynamics, 3, 305–336, https://doi.org/10.5194/wcd-3-305-2022, 2022.

Lejenäs, H.: Characteristics of northern hemisphere blocking as determined from a long time series of observational data, Tellus A, 35, 350–362, https://doi.org/10.3402/tellusa.v35i5.11446, 1983.

https://doi.org/10.5194/egusphere-2025-6306
Preprint. Discussion started: 28 December 2025

Liu, Z. and Wang, L.: Blocking diversity causes distinct roles of diabatic heating in the Northern Hemisphere, Nature Communications, 16, 5613, https://doi.org/10.1038/s41467-025-60811-4, https://www.nature.com/articles/s41467-025-60811-4, 2025.

Lubis, S. W., Harrop, B. E., Lu, J., Leung, L. R., Chen, Z., Huang, C. S. Y., and Omrani, N.-E.: Cloud radiative effects significantly increase wintertime atmospheric blocking in the Euro-Atlantic sector, Nature Communications, 16, 9763, https://doi.org/10.1038/s41467-025-64672-9, https://www.nature.com/articles/s41467-025-64672-9, 2025.

Luo, D., Cha, J., Zhong, L., and Dai, A.: A nonlinear multiscale interaction model for atmospheric blocking: The eddy-blocking matching mechanism, Quarterly Journal of the Royal Meteorological Society, 140, 1785–1808, https://doi.org/10.1002/qj.2337, 2014.

Maddison, J. W., Catto, J. L., Hanna, E., Luu, L. N., and Screen, J. A.: Missing Increase in Summer Greenland Blocking in Climate Models, Geophysical Research Letters, 51, e2024GL108 505, https://doi.org/https://doi.org/10.1029/2024GL108505, https://agupubs.onlinelibrary.wiley.com/doi/abs/10.1029/2024GL108505, e2024GL108505 2024GL108505, 2024.

Madonna, E., Wernli, H., Joos, H., and Martius, O.: Warm Conveyor Belts in the ERA-Interim Dataset (1979-2010). Part I: Climatology and Potential Vorticity Evolution, Journal of Climate, 27, 3 – 26, https://doi.org/10.1175/JCLI-D-12-00720.1, 2014.

Martineau, P., Nakamura, H., Yamamoto, A., and Kosaka, Y.: Baroclinic Blocking, Geophysical Research Letters, 49, e2022GL097 791, https://doi.org/10.1029/2022GL097791, 2022.

Michel, C. and Rivière, G.: The link between rossby wave breakings and weather regime transitions, Journal of the Atmospheric Sciences, 68, 1730–1748, https://doi.org/10.1175/2011JAS3635.1, 2011.

Michelangeli, P. A., Vautard, R., and Legras, B.: Weather regimes: recurrence and quasi stationarity, https://doi.org/10.1175/1520-0469(1995)052<1237:WRRAQS>2.0.CO;2, 1995.

Miller, D. E. and Wang, Z.: Northern Hemisphere Winter Blocking: Differing Onset Mechanisms across Regions, Journal of the Atmospheric Sciences, pp. 1–38, https://doi.org/10.1175/jas-d-21-0104.1, 2022.

Nakamura, H. and Wallace, J. M.: Observed Changes in Baroclinic Wave Activity during the Life Cycles of Low-Frequency Circulation Anomalies, Journal of Atmospheric Sciences, 47, 1100 – 1116, https://doi.org/10.1175/1520-0469(1990)047<1100:OCIBWA>2.0.CO;2, 1990.

Nakamura, H. and Wallace, J. M.: Synoptic Behavior of Baroclinic Eddies during the Blocking Onset, Monthly Weather Review, 121, 1892 – 1903, https://doi.org/10.1175/1520-0493(1993)121<1892:SBOBED>2.0.CO;2, 1993.

Nakamura, N. and Huang, C. S.: Atmospheric blocking as a traffic jam in the jet stream, Science, 361, 42–47, https://doi.org/10.1126/science.aat0721, 2018.

Orlanski, I. and Sheldon, J. P.: Stages In the Energetics of Baroclinic Systems, Tellus, 47, 605–628, https://doi.org/10.1034/j.1600-0870.1995.00108.x, 1995.

Osman, M., Beerli, R., Büeler, D., and Grams, C. M.: Multi-model assessment of sub-seasonal predictive skill for year-round Atlantic–European weather regimes, Quarterly Journal of the Royal Meteorological Society, 149, 2386–2408, https://doi.org/10.1002/qj.4512, 2023.

Petoukhov, V., Rahmstorf, S., Petri, S., and Schellnhuber, H. J.: Quasiresonant amplification of planetary waves and recent Northern Hemisphere weather extremes, Proceedings of the National Academy of Sciences, 110, 5336–5341, https://doi.org/10.1073/pnas.1222000110, 2013.

Pfahl, S., Schwierz, C., Croci-Maspoli, M., Grams, C. M., and Wernli, H.: Importance of latent heat release in ascending air streams for atmospheric blocking, Nature Geoscience, 8, 610–614, https://doi.org/10.1038/ngeo2487, 2015.

https://doi.org/10.5194/egusphere-2025-6306
Preprint. Discussion started: 28 December 2025

Pinheiro, M. C., Ullrich, P. A., and Grotjahn, R.: Atmospheric blocking and intercomparison of objective detection methods: Flow field characteristics, Climate Dynamics, 53, 4189–4216, https://doi.org/10.1007/S00382-019-04782-5/TABLES/8, 2019.

Polster, C. and Wirth, V.: The Onset of a Blocking Event as a "Traffic Jam": Characterization with Ensemble Sensitivity Analysis, Journal of the Atmospheric Sciences, 80, 1681 – 1699, https://doi.org/10.1175/JAS-D-21-0312.1, https://journals.ametsoc.org/view/journals/atsc/80/7/JAS-D-21-0312.1.xml, 2023.

Quinting, J. F. and Grams, C. M.: Toward a Systematic Evaluation of Warm Conveyor Belts in Numerical Weather Prediction and Climate Models. Part I: Predictor Selection and Logistic Regression Model, Journal of the Atmospheric Sciences, 78, 1465 – 1485, https://doi.org/10.1175/JAS-D-20-0139.1, 2021.

Quinting, J. F. and Grams, C. M.: EuLerian Identification of ascending AirStreams (ELIAS 2.0) in numerical weather prediction and climate models – Part 1: Development of deep learning model, Geoscientific Model Development, 15, 715–730, https://doi.org/10.5194/gmd-15-715-2022, 2022.

Quinting, J. F. and Vitart, F.: Representation of synoptic-scale Rossby wave packets and blocking in the S2S prediction project database, Geophysical Research Letters, 46, 1070–1078, https://doi.org/10.1029/2018GL081381, 2019.

Quinting, J. F., Grams, C. M., Oertel, A., and Pickl, M.: EuLerian Identification of ascending AirStreams (ELIAS 2.0) in numerical weather prediction and climate models – Part 2: Model application to different datasets, Geoscientific Model Development, 15, 731–744, https://doi.org/10.5194/gmd-15-731-2022, 2022.

Rex, D. F.: Blocking Action in the Middle Troposphere and its Effect upon Regional Climate, Tellus, 2, 196–211, https://doi.org/10.1111/j.2153-3490.1950.tb00331.x, 1950.

Riemer, M. and Jones, S. C.: Interaction of a tropical cyclone with a high-amplitude, midlatitude wave pattern: Waviness analysis, trough deformation and track bifurcation, Quarterly Journal of the Royal Meteorological Society, 140, 1362–1376, https://doi.org/10.1002/qj.2221, 2014.

Riemer, M., Baumgart, M., and Eiermann, S.: Cyclogenesis Downstream of Extratropical Transition Analyzed by Q-Vector Partitioning Based on Flow Geometry, Journal of the Atmospheric Sciences, 71, 4204–4220, https://doi.org/10.1175/JAS-D-14-0023.1, 2014.

Röthlisberger, M., Martius, O., and Wernli, H.: Northern Hemisphere Rossby Wave Initiation Events on the Extratropical Jet—A Climatological Analysis, J. Climate, 31, 743–760, https://doi.org/10.1175/JCLI-D-17-0346.1, 2018.

Schwierz, C., Croci-Maspoli, M., and Davies, H. C.: Perspicacious indicators of atmospheric blocking, Geophysical Research Letters, 31, https://doi.org/10.1029/2003GL019341, 2004.

Shutts, G. J.: The propagation of eddies in diffluent jetstreams: Eddy vorticity forcing of 'blocking' flow fields, Quarterly Journal of the Royal Meteorological Society, 109, 737–761, https://doi.org/10.1002/qj.49710946204, 1983.

Steinfeld, D. and Pfahl, S.: The Role of Latent Heating in Atmospheric Blocking Dynamics: A Global Climatology, Climate Dynamics, https://doi.org/10.1007/s00382-019-04919-6, 2019.

Steinfeld, D., Boettcher, M., Forbes, R., and Pfahl, S.: The sensitivity of atmospheric blocking to upstream latent heating – numerical experiments, Weather and Climate Dynamics, 1, 405–426, https://doi.org/10.5194/wcd-1-405-2020, https://wcd.copernicus.org/articles/1/405/2020/, 2020.

Suitters, C. C., Martínez-Alvarado, O., Hodges, K. I., Schiemann, R. K. H., and Ackerley, D.: Transient anticyclonic eddies and their relationship to atmospheric block persistence, Weather and Climate Dynamics, 4, 683–700, https://doi.org/10.5194/wcd-4-683-2023, 2023.

https://doi.org/10.5194/egusphere-2025-6306
Preprint. Discussion started: 28 December 2025

Sumner, E. J.: A study of blocking in the Atlantic-European of the northern hemisphere, Quarterly Journal of the Royal Meteorological Society, 80, 402–416, https://doi.org/https://doi.org/10.1002/qj.49708034510, https://rmets.onlinelibrary.wiley.com/doi/abs/10.1002/qj.49708034510, 1954.

Teubler, F. and Riemer, M.: Dynamics of Rossby Wave Packets in a Quantitative Potential Vorticity–Potential Temperature Framework, Journal of the Atmospheric Sciences, 73, 1063–1081, https://doi.org/10.1175/JAS-D-15-0162.1, 2016.

Teubler, F. and Riemer, M.: Potential-Vorticity Dynamics of Troughs and Ridges within Rossby Wave Packets during a 40-Year Reanalysis Period, Weather and Climate Dynamics, 2, 535–559, https://doi.org/10.5194/wcd-2-535-2021, 2021.

Teubler, F., Riemer, M., Polster, C., Grams, C. M., Hauser, S., and Wirth, V.: Similarity and variability of blocked weather-regime dynamics in the Atlantic–European region, Weather and Climate Dynamics, 4, 265–285, https://doi.org/10.5194/wcd-4-265-2023, 2023.

Vautard, R.: Multiple weather regimes over the North Atlantic: analysis of precursors and successors, https://doi.org/10.1175/1520-0493(1990)118<2056:MWROTN>2.0.CO;2, 1990.

Vishnupriya, S., Sprenger, M., Joos, H., and Wernli, H.: The interaction of warm conveyor belt outflows with the upper-level waveguide: a four-type climatological classification, Weather and Climate Dynamics, 6, 1195–1219, https://doi.org/10.5194/wcd-6-1195-2025, https://wcd.copernicus.org/articles/6/1195/2025/, 2025.

Wandel, J., Büeler, D., Knippertz, P., Quinting, J. F., and Grams, C. M.: Why Moist Dynamic Processes Matter for the Sub-Seasonal Prediction of Atmospheric Blocking Over Europe, Journal of Geophysical Research: Atmospheres, 129, e2023JD039 791, https://doi.org/doi.org/10.1029/2023JD039791, 2024.

Wernli, H.: A Lagrangian-based analysis of extratropical cyclones. II: A detailed case-study, Quarterly Journal of the Royal Meteorological Society, 123, 1677–1706, https://doi.org/10.1002/qj.49712354211, 1997.

Wirth, V., Riemer, M., Chang, E. K., and Martius, O.: Rossby wave packets on the midlatitude waveguide-A review, Monthly Weather Review, 146, 1965–2001, https://doi.org/10.1175/MWR-D-16-0483.1, 2018.

Woollings, T., Barriopedro, D., Methven, J., Son, S. W., Martius, O., Harvey, B., Sillmann, J., Lupo, A. R., and Seneviratne, S.: Blocking and its Response to Climate Change, Current Climate Change Reports, 4, 287–300, https://doi.org/10.1007/s40641-018-0108-z, 2018.

Yamazaki, A. and Itoh, H.: Selective absorption mechanism for the maintenance of blocking, Geophysical Research Letters, 36, 4–7, https://doi.org/10.1029/2008GL036770, 2009.